



Production of krypton and xenon isotopes in thick stony and iron targets isotropically irradiated with 1600 MeV protons

E. GILABERT^{1*}, B. LAVIELLE¹, R. MICHEL², I. LEYA^{2,3}, S. NEUMANN² AND U. HERPERS⁴

¹LCNAB, UMR 5084, C.E.N. Bordeaux-Gradignan, BP 120, F-33175 Gradignan, France

²Center for Radiation Protection and Radioecology, University of Hannover, D-30167 Hannover, Germany

³Institute for Isotope Geology and Mineral Resources, ETH Zürich, CH-8092 Zürich, Switzerland

⁴Department of Nuclear Chemistry, University of Cologne, D-50674 Cologne, Germany

*Correspondence author's e-mail address: gilabert@cenbg.in2p3.fr

(Received 2001 July 23; accepted in revised form 2002 April 3)

Abstract—Two spherical targets made of gabbro with a radius of 25 cm and of steel with a radius of 10 cm were irradiated isotropically with 1600 MeV protons at the SATURNE synchrotron at Laboratoire National Saturne (LNS)/CEN Saclay, in order to simulate the production of nuclides in meteorites induced by galactic cosmic-ray protons in space. These experiments supply depth-dependent production rate data for a wide range of radioactive and stable isotopes in up to 28 target elements. In this paper, we report results for ⁷⁸Kr, ^{80–86}Kr isotopes in Rb, Sr, Y and Zr and for ¹²⁴Xe, ¹²⁶Xe, ^{128–132}Xe, ¹³⁴Xe, ¹³⁶Xe isotopes in Ba and La. Krypton and xenon concentrations have been measured at different depths in the spheres by using conventional mass spectrometry. Based on Monte-Carlo techniques, theoretical production rates are calculated by folding depth-dependent spectra of primary and secondary protons and secondary neutrons with the excitation functions of the relevant nuclear reactions. The comparison of the model calculation results with experimental data in the thick target experiments performed at LNS and previously at CERN have allowed adjustments of the poorly known excitation functions of neutron-induced reactions. Thus, for the two experiments at SATURNE, excellent agreement is obtained between experimental and calculated production rates for most Kr and Xe isotopes in all investigated target elements. Only Xe production in Ba in the gabbro is underestimated by the calculations by ~25%. This work validates the approach of the thin-target model calculations of cosmogenic nuclide production rates in the attempt of modeling the interaction of galactic cosmic-ray protons with stony and iron meteorites in space as well as with lunar samples.

INTRODUCTION

The interaction of galactic cosmic rays (GCR) and of solar cosmic rays (SCR) with matter produces a large variety of stable and radioactive nuclides, so-called cosmogenic nuclides. In meteorites, more than 45 cosmogenic nuclides have been studied so far, by using different techniques such as conventional mass spectrometry for noble gases (He, Ne, Ar, Kr and Xe), accelerator mass spectrometry (AMS) for long-lived radionuclides (¹⁰Be, ¹⁴C, ²⁶Al, ³⁶Cl, ⁴¹Ca, ⁶⁰Fe, ⁵⁹Ni, ⁵³Mn and ¹²⁹I) and γ -spectrometry for radionuclides with short or long half-lives.

Cosmogenic nuclides in extraterrestrial matter give information on the irradiated bodies (*e.g.*, exposure age, size and shape erosion and ablation losses in the terrestrial atmosphere) and on the cosmic radiation itself such as composition, spectral distribution and intensity. However, interpretation of the measurements in meteorites is often complex and can be significantly improved by using reliable models capable of describing the depth and size dependence

of the cosmogenic production induced by interactions of high-energy particles with solid bodies in space. To develop such models, several simulation experiments under controlled conditions (Michel *et al.*, 1985, 1989, 1993a,b, 1995; Leya *et al.*, 2000a) were performed over the last 20 years using energetic proton beams in order to simulate GCR and SCR interactions with extraterrestrial matter. These experiments have already generated a large number of depth profiles of nuclides produced in a variety of target elements in spherical thick targets of several sizes and chemical compositions irradiated with incident particles of different energy (Michel *et al.*, 1993a,b). Results of simulation experiments and model calculations have been published (Leya *et al.*, 2000a,b), including most long-lived cosmogenic radionuclides (¹⁰Be, ¹⁴C, ²⁶Al, ³⁶Cl, ⁵³Mn) and the light noble gases (^{3,4}He, ^{20,21,22}Ne, ^{36,38}Ar). The interaction model calculations demonstrate the ability to describe quantitatively the production rate depth dependence of the investigated isotopes in stony meteorites for a large range of sizes.

In this paper, we report the systematic study of Kr and Xe production in a set of simulation experiments of GCR interaction with stony and iron meteorites, performed at SATURNE with 1600 MeV protons. New Kr results from a previous experiment performed at CERN with 600 MeV are also presented. These later data complete the measurements already published by Michel *et al.* (1989) and Leya *et al.* (2000a) for light noble gases and radionuclides.

Cosmogenic Kr and Xe components are detectable in extraterrestrial matter when the amounts of trapped and radiogenic noble gases are not too large (Eberhardt *et al.*, 1966). These cosmogenic nuclides provide good sensors of the exposure history of meteorites and of lunar samples. In particular, the ^{81}Kr -Kr dating method proposed by Marti (1967) and Eugster *et al.* (1967) leads to a reliable determination of irradiation ages, in spite of the difficult problem of measuring a few 10^5 atoms of ^{81}Kr per gram of meteorite. As shown for the chondrites Saint-Séverin (Lavielle and Marti, 1988) and Knyahinya (Lavielle *et al.*, 1997), the cosmogenic ratio $^{78}\text{Kr}/^{83}\text{Kr}$ can be used as a shielding depth indicator in preference to the ratio $^{22}\text{Ne}/^{21}\text{Ne}$. In this way, measurements of isotopic abundances of Kr lead to a consistent shielding-corrected dating method. Because of the generally large abundances of trapped and radiogenic components of Xe relative to the cosmogenic component in meteorites, the determination of an exposure age using Xe isotopes is less accurate than the ^{81}Kr -Kr method. However in lunar samples where the concentrations of trapped Xe are relatively low, the $^{131}\text{Xe}/^{124}\text{Xe}$ ratio is known to represent a sensitive indicator of the shielding depth of the samples (Eugster *et al.*, 1986).

The main target elements for the production of Kr by nuclear reactions in extraterrestrial matter are Rb, Sr, Y, and Zr, all present in trace amounts. For Xe, the main target elements are Ba and rare earth elements. Most of the elements present in extraterrestrial matter from which almost the entire Kr and Xe concentrations are produced were investigated in the LNS172 simulation experiment. Quite distinct nuclear reactions are involved for the Kr and Xe production in these target elements, including for example spallation reactions induced by high-energy protons as well as reactions with low-energy secondary neutrons. From such experiments, information concerning excitation functions of neutron-induced reactions can be derived by comparing measured concentrations and production calculations and by using an iterative approach (Leya *et al.*, 2000a). Due to the difficulty of obtaining monochromatic neutron beams, experimental excitation functions are not available for Kr and Xe for incident neutrons with energies above 25 MeV. This is one of the reasons why these Kr and Xe results are important for validating and improving model calculations. Moreover, they also permit verification of some of the assumptions based on semi-empirical calibrations generally made for the determination of production rates of cosmogenic Kr and Xe.

This work is a part of large investigation of the depth dependence of cosmic-ray produced isotopes in meteorites and

lunar rocks. Studies of the Kr and Xe production in extraterrestrial material irradiated by realistic cosmic-ray spectrum are in progress.

EXPERIMENTAL METHOD

Gabbro Sphere Irradiated with 1600 MeV Protons

This experiment was performed with an artificial meteoroid with a radius of 25 cm made of gabbro. Gabbro is a natural rock with a density of 3.0 g/cm^3 and a chemical composition in the range of the bulk composition of the different stony meteorite classes. Its mean mass number (22.2) and its mean atomic number (11.0) match those of stony meteorites within 10%. The artificial meteoroid was irradiated with 1600 MeV protons in the SATURNE synchrotron at the Laboratoire National Saturne (LNS) at Saclay, France from 1990 March 28 to 1990 April 8. A complex movement of the thick target during irradiation ensured an isotropic irradiation. The irradiation was performed at the maximum beam intensity for 2 weeks. The resulting fluence was necessary to obtain measurable amounts of stable and long-lived products. The integrated flux of primary protons through the gabbro was measured *via* the ^{22}Na activity in a large Al foil that followed the different movements of the sphere. The total time of irradiation was 257 h and the artificial meteoroid received a primary proton fluence of $(1.322 \pm 0.013) \times 10^{14} \text{ cm}^{-2}$, which is roughly equivalent to 1.6 Ma of cosmic-ray exposure. All details of the experiment have previously been reported (Lüpke, 1993; Michel *et al.*, 1993a, 1994, 1995; Leya *et al.*, 2000a). The artificial meteoroid consisted of two perpendicular cores that contained more than 1600 small pure element samples and some suitable chemical compounds, minerals and degassed meteoritic materials. These materials covered more than 25 target elements. For each target material up to 10 different samples were located at different depths in the thick target. After irradiation, the samples were removed and distributed among the collaborating laboratories that analyzed them using different experimental techniques to investigate the produced radioactive and stable residual nuclides.

Iron Sphere Irradiated with 1600 MeV Protons

In order to simulate the interactions of galactic protons with iron meteoroids, an artificial iron meteoroid made of steel (99% Fe) with a diameter of 20 cm was isotropically irradiated with 1600 MeV protons at the Saturn cyclotron between 1992 November 27 and 1992 December 7 (Michel *et al.*, 1993b; Leya, 1997). The sphere was equipped with three perpendicular cores containing more than 900 individual targets that covered most of the elements investigated in the "gabbro 1600 MeV" experiment. During the 125.7 h of irradiation, the artificial meteoroid received a proton fluence of $(2.453 \pm 0.024) \times 10^{14} \text{ cm}^{-2}$, which is roughly equivalent to 3 Ma exposure of a meteoroid in space.

More details of these experiments were presented by Leya *et al.* (2000a).

Gabbro Sphere Irradiated with 600 MeV Protons

The experiment was performed at CERN on 1984 November 22 (Dragovitsch, 1987; Michel *et al.*, 1989). The scientific goals and the experimental approach were similar to those defined in the more recent simulation experiments performed at SATURNE. The irradiation conditions were practically the same, except for the radius of the sphere (15 cm) and the energy of the incident proton beam (600 MeV). The total proton fluence received by the sphere was $(5.94 \pm 0.02) \times 10^{14} \text{ cm}^{-2}$. Details of the experiment were reported by Michel *et al.* (1989).

After the irradiation, the individual targets were distributed to the collaborating laboratories where the different nuclides were investigated by x-ray and γ -ray spectrometry and by conventional and AMS.

Target Preparation

Krypton was analyzed in thin Zr and Y foils, in SrF₂ crystals and in Rb₂SO₄ compacted powder. Xenon was analyzed in Ba glasses, in LaF₃ compacted powder and in LaF₃ crystals. For each investigated element, 8 or 10 targets were placed evenly spaced inside the sphere in two perpendicular directions. Yttrium and Zr targets had the highest purity available from Goodfellow Metals, usually better than 99.99%. Crystals of SrF₂ from CRISTAL-TEC (Grenoble, France) were selected as Sr targets. Rubidium targets were prepared from high-purity Rb₂SO₄ powder from Alfa Products (99.9%). The powder was first degassed under vacuum conditions at 400 °C for 40 min in a container made of Pyrex. After sealing the container, the powder was transferred in a glove box kept under nitrogen atmosphere in order to avoid noble gas contamination from air. Then, it was compacted in a cast of 1.6 mm interior diameter by applying a pressure of 4 tons while operating in a nitrogen atmosphere. The thus produced pills were baked at 600 °C

again in a nitrogen atmosphere for hours to improve their mechanical properties. For preparing La targets, we followed the same procedure as for Rb₂SO₄ powder using high-purity LaF₃ powder (from Alfa Products with 99.9% of purity). However, the degassing time at 400 °C was increased to 5 h. Barium glass targets containing 0.4021 g/g of Ba were obtained from Schott (Mainz, Germany) and crystals of LaF₃ from Merck products. Characteristics are summarized in Table 1.

MASS SPECTROMETRY MEASUREMENTS

Krypton and Xe concentrations in Sr, Rb, Y, Zr, Ba and La targets were measured at the Laboratoire de Chimie Nucléaire Analytique et Bioenvironnementale (LCNAB). The mass spectrometer utilized is a 12 cm radius and 60° magnetic sector Micromass 12 type from vacuum generator (VG) equipped with an electron multiplier, microcomputer assisted peak switching and a data storage unit. For each noble gas measurement, we used only 30–50% of the target material available. Therefore, duplicate measurements were performed to ensure the reproducibility of the noble gas results. Including target blank measurements, ~150 samples were analyzed in this work.

After loading in the storage arm of the extraction system, the samples were heated for several days at 80 °C under 10⁻⁸ mbar pressure to remove atmospheric gases trapped on the surface.

To melt the samples, we used two types of crucibles depending on the melting point of the targets and on the weight of the samples. Type 1 is a Mo crucible heated to a temperature of ~1900 °C by electron bombardment using an accelerating voltage of 1500 V. Type 2 is a stainless steel crucible heated by a resistor. It was used to analyze big samples of Ba glass and Rb₂SO₄ with 1 g weight and a melting point below 1150 °C. Yttrium, Zr, SrF₂ and LaF₃ were melted in the crucible of type 1. Yttrium targets were analyzed using two temperature steps (700 and 1600 °C). The purpose of the first step was to remove possible air contamination from the surface trapped by oxidation. The Kr released at low temperature showed almost no atmospheric contamination. It represented ~6% of the total

TABLE 1. Characteristics and properties of the targets used in the sphere.

Target	Zr	Y	SrF ₂	Rb ₂ SO ₄	LaF ₃	LaF ₃	Ba glass
Physical form	Foil	Foil	Crystal	Compacted powder	Compacted powder	Crystal	Glass
Manufacturer	Goodfellow Metals	Goodfellow Metals	Cristal Tec	Alfa Products	Alfa Products	Merck	Schott
Diameter (mm)	15.9	15.9	15.0	15.9	15.9	8.0	15.9
Thickness (mm)	0.25	0.1	1.0	3.0	3.0	1.0	3.2
Typical weight (mg)	325	90	900	1250	1000	300	2000
Fraction of the element	1.00	1.00	0.6975	0.6404	0.7092	0.7092	0.4013
Melting point (°C)	1852	1523	1450	1060	1493	1493	<1000

amount extracted from the sample after melting. For Rb targets we used also two temperature steps: 450 and 1100 °C. Only ~4% of the gas was released at low temperature. This small release at 450 °C confirmed the procedure selected for sample preparation from powder that led to a good gas retention property and to the lack of any gas loss during the irradiation time. Krypton was extracted from Sr and Zr using single step heating at 1600 and 1900 °C, respectively. Similarly, Xe was extracted from Ba and La at 1150 or 1600 °C, respectively. For each target, a final heating was done at a temperature of at least 100 °C above the melting point to verify the complete release of the gas. Generally, during this last heating, the amount of noble gas released was small for most samples (<1%). It reached ~3% of the total gas for one of the Zr targets.

Extracted gases were cleaned successively with Ti sponges, Al-Zr getters (SAES; working at 450 °C), Pd and Ti powders at stepwise decreasing temperature (from 700 to 350 °C) in our all-metal system of small volume. During Rb and La target analysis, heavier noble gases (Kr and Xe) were cryogenically separated from Ar on charcoal at -125 °C in order to lower the gas pressure in the mass spectrometer during Kr analyses. A relatively large concentration of ⁴⁰Ar due to atmospheric contamination of the targets can induce memory effects for Kr isotopes and can also increase the background of the mass spectrometer. Both effects can affect the quality of the measurements. On the other hand, no separation was necessary for Y, Zr, Sr and Ba targets for which atmospheric contamination was always very low.

Calibration

For the gabbro experiments (600 and 1600 MeV), we used a standard calibration procedure. For the iron sphere, we always used an isotopic dilution calibration procedure. Both procedures are described below.

For the standard calibration, we utilized a special mixture of Kr and Xe with an isotopic composition different from that of air and of that currently measured in irradiated targets. The Kr and Xe contents in the calibration system were regularly checked by using a very precise isotopic dilution procedure similar to that described below but using an air standard pipette. Standard calibrations were adopted to measure sensitivity and mass discrimination of the mass spectrometer after or prior to target analysis. The reproducibility was ~7% and represents the largest source of uncertainties. The Kr mass discrimination was constant for the duration of the complete set of target analyses with a value of $0.7 \pm 0.2\%$ /amu (amu = atomic mass unit). For Xe the mass discrimination shifted from 0.70 ± 0.15 to $0.3 \pm 0.1\%$ /amu after a change in the tuning of the ion source.

Special care was taken regarding the isotope dilution calibration procedure to improve the precision and the reproducibility of the absolute Kr and Xe concentration measurements. Extracted gases from the targets were split into several well-defined volume fractions. One fraction was first

analyzed to determine the isotopic composition of the gas produced in the target by the irradiation. Depending on the amount of gas produced in the target, several measurements of the isotopic composition were made independently by using different aliquots in order to increase the accuracy of the measurement. Then, an aliquot of the remaining gas kept in a volume known with high precision, typically better than 0.5%, was mixed with a calibrated gas sample known with a precision better than 1.5%. This latter gas has an isotopic composition different from both air and that found in the irradiated targets. Isotopic ratios measured in the mixture allowed a precise determination of the concentration of the gas fraction coming from the target relative to the amount added for calibration. The particular advantage of this method is to allow measurement of absolute concentrations without being affected by any variation of sensitivity of the mass spectrometer because calibration and isotopic analysis of the investigated sample are performed simultaneously. Such variations represent in general the major sources of experimental uncertainties in concentration measurements of noble gases by mass spectrometry. Finally, the calibration system is regularly checked by using an isotopic dilution procedure with a calibrated air pipette.

Absolute uncertainties of concentrations determined by isotope dilution do not exceed 3%, including all sources of uncertainty: reproducibility of the measurement, uncertainties of the determination of the isotopic compositions, uncertainties of the pipette sample and of the gas fractions. The isotopic dilution technique, which is based only on isotopic ratio measurements, reduced uncertainties on the concentration determination by a factor of 2 to 5 relative to the standard procedure.

Blanks

Data are corrected taking into account both system blanks and target blanks.

System Blanks—System blanks correspond to the gas released by the line used for the extraction and the preparation of the gas sample. In particular, hot blanks were regularly measured with the two types of crucibles used in this work. In general, the measured quantities were very small compared to the extracted gases from the samples. Blanks have air composition and typical blank concentrations are 1×10^{-12} cm³/g STP for ⁸³Kr, and $<1 \times 10^{-13}$ cm³/g STP for ¹³²Xe.

Target Blanks—Targets blanks correspond to the gas fraction contained in the target material itself. They were measured in not-irradiated samples. During these experiments we used several types of targets containing different amounts of air contamination. Foils (Y, Zr), crystals (SrF₂, LaF₃) and glass (Ba) have the lowest air content and compacted powder (Rb₂SO₄, LaF₃) show much larger contamination, probably trapped mainly during the production of the targets. Typical ⁸³Kr blank concentrations are (in units of 10⁻¹² cm³/g STP): 6, 5, <0.1 and, 250 for Y, Zr, SrF₂, Rb₂SO₄ targets, respectively.

For ^{132}Xe , typical blank concentrations are (in units of 10^{-12} cm³/g STP): 17, 52, 5, for Ba (glass), LaF₃ (powder), and LaF₃ (crystal), respectively. In targets prepared by compaction of powder, the largest corrections were required, corresponding to ~4.0% for ^{83}Kr in Rb₂SO₄ and ~8% for ^{132}Xe in LaF₃. We observed that blank concentrations could vary by a factor of 3 in different samples. A systematic study of this atmospheric contamination allowed us to establish two three-isotope correlations for Rb and La targets, respectively, using the ratios $^{36}\text{Ar}/^{132}\text{Xe}$, $^{36}\text{Ar}/^{84}\text{Kr}$ and $^{84}\text{Kr}/^{132}\text{Xe}$. Blank corrections in irradiated Rb and La targets were determined by using the established correlation plots and the measured concentrations of ^{36}Ar and ^{132}Xe in Rb targets and of ^{36}Ar and ^{84}Kr in La targets that are essentially of atmospheric composition.

For the 600 MeV experiment in gabbro, we analyzed the Y target series without any blank target being available. Air contamination for these measurements was taken to be the mean value obtained in other Y targets.

Experimental Results

Tables 2 and 3 present the measured Kr and Xe concentrations and the corresponding isotopic ratios for Zr, Y, Sr, Rb, Ba and La targets vs. the distance to the center of the artificial meteoroids (gabbros and iron). Reported production rates $P(^{83}\text{Kr})$ and $P(^{126}\text{Xe})$ (in units of 10^{-12} cm³ STP g⁻¹ Ma⁻¹) are calculated using the relation

$$P = J_0 \frac{C}{\Psi} \quad (1)$$

where C is the measured concentration (in units of 10^{-12} cm³ STP g⁻¹) of ^{83}Kr or ^{126}Xe in the iron or in the gabbro sphere experiment. Ψ is the total proton fluence (in units of cm⁻²) received by the spheres during the irradiation and J_0 is the proton flux density normalized to 1 cm⁻² s⁻¹ (3.156×10^{13} cm⁻² Ma⁻¹). All data are corrected for blanks and instrumental mass discrimination. Uncertainties on concentrations and isotopic ratios are standard uncertainties according to ISO (1995) and include all experimental sources of type A and type B uncertainties. For several locations, duplicate analysis were done by splitting the targets in two or three parts in order to verify the reproducibility of the measurements and to improve the precision. Uncertainties on production rates include the uncertainty on the determination of the proton fluences received during the different irradiations.

MODEL CALCULATIONS

Calculation of Particle Fluxes

Monte-Carlo calculations of depth- and size-dependent spectra of primary and secondary nucleons inside the artificial meteoroids were performed using the high-energy transport

code (HETC) (Armstrong and Chandler, 1972) within the HERMES code system (Cloth *et al.*, 1988). HERMES (high-energy radiation Monte-Carlo elaborate system) is a system of Monte-Carlo computer codes which allows us to treat the different physical phenomena which must be considered in computer simulations of radiation transport and interaction problems.

The proton histories were followed down to $E_p = 0.5$ MeV by HETC. Neutrons with energies lower than 15 MeV were submitted to the Monte-Carlo code MORSE-CG (Emmet, 1975) of the HERMES system to perform neutron transport analysis with a coupled neutron gamma library with 100 neutron groups (10^{-4} eV to 15 MeV) derived from the evaluated data base ENDF/B-IV (Kinsey, 1979). There were 29 energy groups for protons between 0.5 MeV and 1600 MeV and 23 groups for neutrons between 15 MeV and 1600 MeV.

For the analysis of the resulting particle spectra the artificial meteoroids were divided into concentric shells with a thickness of 2.5 cm (gabbro sphere, $R = 25$ cm), 1.0 cm (gabbro sphere, $R = 15$ cm), and 0.5 cm (steel sphere), respectively. For all these shells the spectra of primary protons and of secondary protons and neutrons were calculated and normalized to an integral particle flux of primary 1.6 or 0.6 GeV protons of 1 cm⁻² s⁻¹ seen by the artificial meteoroids. A presentation of the results of these calculations is omitted here since they were reported and discussed in detail by Michel *et al.* (1989) and Leya *et al.* (2000a).

Calculated Production Rates in the Spheres: *A Priori* and *A Posteriori* Calculations

Theoretical production rates were derived by folding the calculated proton and neutron spectra with the thin-target cross sections of the underlying nuclear reactions. We followed exactly the procedure described in detail by Leya *et al.* (2000a). Thus, first *a priori* model calculations were performed on the basis of all present knowledge about the cross sections of the underlying nuclear reactions. Then improved neutron cross sections were derived by unfolding from the thick-target production rates which then provided the basis for improved *a posteriori* calculations of production rates. We shall describe here only those details relevant for model calculation of the production rates of Kr and Xe, otherwise we refer to Leya *et al.* (2000a). For more details of the model calculations see Neumann (1999).

The excitation functions for the proton-induced reactions were taken in the case of krypton from the work of Gilabert *et al.* (1998) and Regnier *et al.* (1982) and, in the case of Xe, from Prescher *et al.* (1991) and Mathews *et al.* (1994) and references therein. Gaps in the experimental excitation functions were closed by interpolations based on the shapes of theoretical cross sections for these reactions calculated by the AREL code (Blann, 1994, pers. comm.), which is an improved version of the ALICE Livermore 82 code (Blann and Bisplinghoff,

TABLE 2a. Measured concentrations, production rates of ^{83}Kr and Kr isotopic ratios vs. distance to the center in Rb, Sr, Y, and Zr targets irradiated with 1600 MeV protons in the gabbro sphere ($R = 25$ cm).

Target	r^\dagger (g/cm ²)	^{83}Kr (10^{-12} cm ³ /g)	$P(^{83}\text{Kr})^*$	$^{78}\text{Kr}/^{83}\text{Kr}$	$^{80}\text{Kr}/^{83}\text{Kr}$	$^{81}\text{Kr}/^{83}\text{Kr}$	$^{82}\text{Kr}/^{83}\text{Kr}$	$^{84}\text{Kr}/^{83}\text{Kr}$	$^{85}\text{Kr}/^{83}\text{Kr}$	$^{86}\text{Kr}/^{83}\text{Kr}$
Rb	16.8	12694 ± 1092	3030 ± 301	0.1002 ± 0.0012	0.4129 ± 0.0031	0.4582 ± 0.0044	0.6985 ± 0.0031	1.2675 ± 0.0319	0.05326 ± 0.00052	0.04801 ± 0.01263
Rb	24.3	12401 ± 1054	2960 ± 292	0.1002 ± 0.0012	0.4115 ± 0.0031	0.4557 ± 0.0045	0.6973 ± 0.0032	1.2739 ± 0.0331	0.05299 ± 0.00053	0.05135 ± 0.01310
Rb	32.1	12156 ± 1043	2902 ± 288	0.1008 ± 0.0012	0.4150 ± 0.0032	0.4579 ± 0.0045	0.6999 ± 0.0031	1.2748 ± 0.0328	0.05298 ± 0.00052	0.05280 ± 0.01299
Rb	39.3	11907 ± 1002	2842 ± 278	0.1022 ± 0.0012	0.4196 ± 0.0032	0.4613 ± 0.0043	0.7033 ± 0.0030	1.2666 ± 0.0311	0.05328 ± 0.00051	0.05163 ± 0.01228
Rb	46.8	11217 ± 950	2678 ± 263	0.1035 ± 0.0012	0.4216 ± 0.0032	0.4642 ± 0.0045	0.7034 ± 0.0031	1.2701 ± 0.0323	0.05322 ± 0.00052	0.05345 ± 0.01275
Rb	54.3	11072 ± 947	2643 ± 262	0.1045 ± 0.0012	0.4234 ± 0.0032	0.4652 ± 0.0044	0.7042 ± 0.0031	1.2551 ± 0.0316	0.05302 ± 0.00051	0.05072 ± 0.01244
Rb	61.8	9891 ± 843	2361 ± 233	0.1075 ± 0.0014	0.4318 ± 0.0039	0.4721 ± 0.0062	0.7109 ± 0.0041	1.2530 ± 0.0464	0.05304 ± 0.00071	0.05276 ± 0.01828
Rb	69.3	9200 ± 787	2196 ± 218	0.1095 ± 0.0015	0.4379 ± 0.0042	0.4756 ± 0.0066	0.7136 ± 0.0043	1.2402 ± 0.0495	0.05341 ± 0.00075	0.05180 ± 0.01945
Sr	14.7	6297 ± 535	1503 ± 148	0.1584 ± 0.0018	0.4995 ± 0.0035	0.5599 ± 0.0026	0.7555 ± 0.0023	0.6209 ± 0.0021	0.03391 ± 0.00020	0.01852 ± 0.00023
Sr	24.0	6004 ± 509	1433 ± 141	0.1690 ± 0.0018	0.5154 ± 0.0034	0.5725 ± 0.0029	0.7658 ± 0.0045	0.6074 ± 0.0033	0.03410 ± 0.00039	0.01703 ± 0.00022
Sr	24.0	6453 ± 550	1540 ± 152	0.1675 ± 0.0017	0.5121 ± 0.0033	0.5725 ± 0.0027	0.7604 ± 0.0050	0.6082 ± 0.0028	0.03388 ± 0.00034	0.01743 ± 0.00023
Sr	24.0	5807 ± 490	1386 ± 136	0.1605 ± 0.0017	0.5046 ± 0.0033	0.5648 ± 0.0028	0.7587 ± 0.0021	0.6188 ± 0.0015	0.03353 ± 0.00023	0.01835 ± 0.00015
Sr	29.7	6260 ± 531	1494 ± 147	0.1637 ± 0.0018	0.5060 ± 0.0032	0.5659 ± 0.0026	0.7583 ± 0.0024	0.6170 ± 0.0020	0.03315 ± 0.00023	0.01855 ± 0.00020
Sr	39.0	6252 ± 531	1493 ± 147	0.1669 ± 0.0016	0.5166 ± 0.0033	0.5771 ± 0.0026	0.7678 ± 0.0018	0.6252 ± 0.0015	0.03405 ± 0.00016	0.01886 ± 0.00013
Sr	39.0	6542 ± 557	1562 ± 154	0.1675 ± 0.0017	0.5170 ± 0.0031	0.5738 ± 0.0024	0.7683 ± 0.0018	0.6230 ± 0.0013	0.03378 ± 0.00015	0.01890 ± 0.00014
Sr	44.7	6056 ± 516	1446 ± 143	0.1641 ± 0.0018	0.5098 ± 0.0031	0.5684 ± 0.0025	0.7612 ± 0.0021	0.6166 ± 0.0017	0.03412 ± 0.00020	0.01882 ± 0.00018
Sr	54.0	5955 ± 505	1422 ± 140	0.1667 ± 0.0020	0.5190 ± 0.0037	0.5748 ± 0.0030	0.7615 ± 0.0025	0.6143 ± 0.0020	0.03360 ± 0.00040	0.01802 ± 0.00019
Sr	60.0	5562 ± 468	1328 ± 130	0.1679 ± 0.0018	0.5192 ± 0.0034	0.5753 ± 0.0027	0.7616 ± 0.0030	0.6152 ± 0.0020	0.03418 ± 0.00037	0.01893 ± 0.00018
Sr	69.0	5020 ± 427	1198 ± 118	0.1757 ± 0.0019	0.5304 ± 0.0035	0.5806 ± 0.0026	0.7683 ± 0.0027	0.6136 ± 0.0020	0.03395 ± 0.00027	0.01881 ± 0.00029
Y	7.2	4686 ± 405	1119 ± 112	0.2317 ± 0.0027	0.5420 ± 0.0034	0.6378 ± 0.0031	0.7854 ± 0.0030	0.3471 ± 0.0019	0.00397 ± 0.00013	0.00307 ± 0.00037
Y	13.8	4615 ± 394	1102 ± 109	0.2301 ± 0.0024	0.5425 ± 0.0038	0.6302 ± 0.0031	0.7831 ± 0.0028	0.3497 ± 0.0017	0.00399 ± 0.00018	0.00383 ± 0.00025

TABLE 2a. *Continued.*

Target	r^\dagger (g/cm ²)	⁸³ Kr (10 ⁻¹² cm ³ /g)	$P(^{83}\text{Kr})^*$	⁷⁸ Kr/ ⁸³ Kr	⁸⁰ Kr/ ⁸³ Kr	⁸¹ Kr/ ⁸³ Kr	⁸² Kr/ ⁸³ Kr	⁸⁴ Kr/ ⁸³ Kr	⁸⁵ Kr/ ⁸³ Kr	⁸⁶ Kr/ ⁸³ Kr
Y	22.5	4708 ±397	1124 ±110	0.2337 ±0.0023	0.5443 ±0.0038	0.6357 ±0.0033	0.7852 ±0.0044	0.3448 ±0.0030	0.00416 ±0.00024	0.00368 ±0.00033
Y	22.5	5020 ±427	1198 ±118	0.2386 ±0.0025	0.5501 ±0.0037	0.6402 ±0.0033	0.7853 ±0.0029	0.3349 ±0.0025	0.00445 ±0.00016	0.00392 ±0.00033
Y	28.8	4578 ±390	1093 ±108	0.2328 ±0.0029	0.5519 ±0.0044	0.6441 ±0.0055	0.7776 ±0.0042	0.3406 ±0.0024	0.00315 ±0.00023	0.00308 ±0.00025
Y	28.8	4608 ±394	1100 ±109	0.2348 ±0.0026	0.5441 ±0.0040	0.6302 ±0.0038	0.7786 ±0.0035	0.3504 ±0.0076	0.00397 ±0.00017	0.00445 ±0.00238
Y	37.5	4396 ±364	1049 ±101	0.2466 ±0.0037	0.5484 ±0.0048	0.6493 ±0.0043	0.7891 ±0.0042	0.3477 ±0.0023	0.00619 ±0.00038	0.00192 ±0.00196
Y	37.5	3720 ±316	888 ±87	0.2390 ±0.0031	0.5518 ±0.0041	0.6409 ±0.0042	0.7885 ±0.0063	0.3454 ±0.0031	0.00393 ±0.00019	0.00201 ±0.00009
Y	44.1	4121 ±338	984 ±94	0.2440 ±0.0028	0.5562 ±0.0034	0.6414 ±0.0032	0.7865 ±0.0040	0.3442 ±0.0025	0.00327 ±0.00019	0.00352 ±0.00040
Y	44.1	4359 ±368	1041 ±102	0.2371 ±0.0024	0.5520 ±0.0036	0.6385 ±0.0027	0.7913 ±0.0040	0.3452 ±0.0022	0.00386 ±0.00013	0.00362 ±0.00028
Y	52.8	4132 ±353	986 ±98	0.2436 ±0.0027	0.5673 ±0.0044	0.6505 ±0.0034	0.7908 ±0.0036	0.3456 ±0.0019	0.00395 ±0.00016	0.00370 ±0.00038
Y	59.1	3969 ±338	947 ±94	0.2454 ±0.0028	0.5585 ±0.0043	0.6406 ±0.0032	0.7873 ±0.0046	0.3446 ±0.0026	0.00352 ±0.00018	0.00221 ±0.00084
Y	68.1	3735 ±319	892 ±88	0.2564 ±0.0047	0.5815 ±0.0056	0.6590 ±0.0037	0.8000 ±0.0049	0.3484 ±0.0022	0.00366 ±0.00014	0.00197 ±0.00019
Y	74.4	3093 ±264	738 ±73	0.2552 ±0.0033	0.5797 ±0.0044	0.6622 ±0.0036	0.7925 ±0.0030	0.3437 ±0.0018	0.00351 ±0.00014	0.00477 ±0.00028
Zr	5.7	3097 ±264	739 ±73	0.2904 ±0.0030	0.5876 ±0.0042	0.6744 ±0.0033	0.8161 ±0.0033	0.2185 ±0.0014	0.00483 ±0.00013	0.00441 ±0.00029
Zr	10.8	3026 ±260	722 ±72	0.2947 ±0.0041	0.5943 ±0.0050	0.6864 ±0.0041	0.8210 ±0.0061	0.2251 ±0.0015	0.00366 ±0.00023	0.00353 ±0.00046
Zr	10.8	3052 ±260	729 ±72	0.2919 ±0.0030	0.5887 ±0.0037	0.6695 ±0.0033	0.8087 ±0.0035	0.2190 ±0.0014	0.00460 ±0.00010	0.00502 ±0.00039
Zr	21.3	3074 ±290	734 ±78	0.2952 ±0.0030	0.5871 ±0.0038	0.6757 ±0.0032	0.8071 ±0.0026	0.2222 ±0.0013	0.00463 ±0.00014	0.00399 ±0.00031
Zr	25.8	3234 ±275	772 ±76	0.2941 ±0.0031	0.5841 ±0.0036	0.6749 ±0.0030	0.8127 ±0.0026	0.2198 ±0.0010	0.00484 ±0.00012	0.00411 ±0.00029
Zr	36.3	3026 ±260	722 ±72	0.2944 ±0.0030	0.5913 ±0.0040	0.6797 ±0.0032	0.8129 ±0.0031	0.2257 ±0.0016	0.00488 ±0.00021	0.00595 ±0.00045
Zr	40.8	2792 ±238	666 ±66	0.2985 ±0.0032	0.5946 ±0.0041	0.6744 ±0.0034	0.8135 ±0.0026	0.2151 ±0.0023	0.00462 ±0.00007	0.00269 ±0.00056
Zr	40.8	2792 ±238	666 ±66	0.2957 ±0.0030	0.5908 ±0.0037	0.6772 ±0.0032	0.8102 ±0.0025	0.2209 ±0.0016	0.00483 ±0.00012	0.00460 ±0.00037
Zr	51.6	2803 ±238	669 ±66	0.3026 ±0.0033	0.6024 ±0.0041	0.6848 ±0.0034	0.8214 ±0.0036	0.2209 ±0.0020	0.00447 ±0.00024	0.00485 ±0.00046

TABLE 2a. *Continued.*

Target	r† (g/cm ²)	⁸³ Kr (10 ⁻¹² cm ³ /g)	P(⁸³ Kr)*	⁷⁸ Kr/ ⁸³ Kr	⁸⁰ Kr/ ⁸³ Kr	⁸¹ Kr/ ⁸³ Kr	⁸² Kr/ ⁸³ Kr	⁸⁴ Kr/ ⁸³ Kr	⁸⁵ Kr/ ⁸³ Kr	⁸⁶ Kr/ ⁸³ Kr
Zr	56.4	2892 ±245	690 ±68	0.3088 ±0.0032	0.6028 ±0.0039	0.6862 ±0.0033	0.8183 ±0.0030	0.2211 ±0.0013	0.00451 ±0.00013	0.00516 ±0.00039
Zr	66.6	2543 ±219	607 ±60	0.3202 ±0.0035	0.6138 ±0.0040	0.6976 ±0.0036	0.8306 ±0.0036	0.2207 ±0.0014	0.00452 ±0.00030	0.00415 ±0.00043
Zr	72.0	2057 ±175	491 ±48	0.3202 ±0.0034	0.6186 ±0.0040	0.7021 ±0.0030	0.8244 ±0.0034	0.2251 ±0.0017	0.00470 ±0.00013	0.00614 ±0.00054
Zr	72.0	2101 ±178	502 ±49	0.3138 ±0.0034	0.6108 ±0.0042	0.6942 ±0.0037	0.8217 ±0.0036	0.2235 ±0.0018	0.00472 ±0.00015	0.00617 ±0.00056

*Production rates in 10⁻¹² cm³/g/Ma normalized to a flux density of primary protons $J_0 = 1 \text{ s}^{-1} \text{ cm}^{-2}$.

†Distance to the center in g/cm² (density of gabbro = 3.0 g/cm³); ⁸⁵Kr is corrected for radioactive decay ($t_{1/2} = 10.7$ years). Errors at 1σ .

TABLE 2b. Measured concentrations, production rates of ⁸³Kr and Kr isotopic ratios vs. distance to the center in Sr, Y, and Zr targets irradiated with 1600 MeV protons in the iron sphere ($R = 10$ cm).

Target	r† (g/cm ²)	⁸³ Kr (10 ⁻¹² cm ³ /g)	P(⁸³ Kr)*	⁷⁸ Kr/ ⁸³ Kr	⁸⁰ Kr/ ⁸³ Kr	⁸¹ Kr/ ⁸³ Kr	⁸² Kr/ ⁸³ Kr	⁸⁴ Kr/ ⁸³ Kr	⁸⁵ Kr/ ⁸³ Kr	⁸⁶ Kr/ ⁸³ Kr
Sr	33.1	12392 ±265	1594 ±87	0.1603 ±0.0013	0.4995 ±0.0022	0.5590 ±0.0017	0.7526 ±0.0017	0.6254 ±0.0061	0.02944 ±0.00090	0.01803 ±0.00198
Sr	41.4	12034 ±245	1548 ±84	0.1626 ±0.0013	0.5024 ±0.0022	0.5615 ±0.0017	0.7546 ±0.0017	0.6312 ±0.0058	0.02897 ±0.00084	0.01996 ±0.00184
Sr	52.1	11247 ±226	1447 ±78	0.1647 ±0.0013	0.5067 ±0.0021	0.5639 ±0.0016	0.7563 ±0.0017	0.6260 ±0.0061	0.03024 ±0.00125	0.01869 ±0.00197
Sr	60.3	10426 ±211	1341 ±72	0.1685 ±0.0014	0.5130 ±0.0022	0.5664 ±0.0018	0.7602 ±0.0017	0.6273 ±0.0065	0.03048 ±0.00068	0.01891 ±0.00214
Sr	76.7	7954 ±166	1023 ±55	0.1780 ±0.0017	0.5309 ±0.0038	0.5852 ±0.0030	0.7662 ±0.0035	0.6386 ±0.0090	0.02842 ±0.00525	0.02124 ±0.00297
Y	32.4	8792 ±185	1131 ±61	0.2326 ±0.0022	0.5418 ±0.0031	0.6317 ±0.0037	0.7786 ±0.0103	0.3529 ±0.0186	0.00445 ±0.00026	0.00270 ±0.00623
Y	42.7	8350 ±182	1074 ±59	0.2396 ±0.0023	0.5553 ±0.0032	0.6554 ±0.0046	0.7910 ±0.0021	0.3261 ±0.0200	0.00792 ±0.00153	-0.00720 ±0.00668
Y	51.5	8009 ±173	1030 ±56	0.2456 ±0.0023	0.5632 ±0.0033	0.6575 ±0.0041	0.8080 ±0.0063	0.3653 ±0.0206	0.00550 ±0.00012	0.00302 ±0.00688
Y	76.2	6089 ±133	783 ±43	0.2691 ±0.0028	0.6055 ±0.0044	0.6950 ±0.0056	0.8407 ±0.0093	0.3855 ±0.0285	0.00649 ±0.00014	0.01561 ±0.00936
Zr	20.1	5850 ±122	753 ±41	0.3000 ±0.0024	0.5952 ±0.0024	0.6818 ±0.0016	0.8144 ±0.0019	0.2170 ±0.0033	0.00558 ±0.00057	0.00173 ±0.00103
Zr	31.7	6009 ±122	773 ±42	0.3041 ±0.0024	0.5992 ±0.0024	0.6828 ±0.0016	0.8153 ±0.0019	0.2182 ±0.0031	0.00399 ±0.00034	0.00180 ±0.00095
Zr	41.1	5820 ±121	749 ±41	0.3056 ±0.0024	0.6022 ±0.0025	0.6853 ±0.0016	0.8170 ±0.0019	0.2170 ±0.0033	0.00497 ±0.00058	0.00209 ±0.00104

TABLE 2b. *Continued.*

Target	r [†] (g/cm ²) (10 ⁻¹² cm ³ /g)	⁸³ Kr	P(⁸³ Kr)*	⁷⁸ Kr/ ⁸³ Kr	⁸⁰ Kr/ ⁸³ Kr	⁸¹ Kr/ ⁸³ Kr	⁸² Kr/ ⁸³ Kr	⁸⁴ Kr/ ⁸³ Kr	⁸⁵ Kr/ ⁸³ Kr	⁸⁶ Kr/ ⁸³ Kr
Zr	51.0	5444 ±112	700 ±38	0.3116 ±0.0025	0.6101 ±0.0026	0.6897 ±0.0020	0.8201 ±0.0020	0.2155 ±0.0034	0.00434 ±0.00095	0.00116 ±0.00107
Zr	51.0	5516 ±133	710 ±39	0.3098 ±0.0025	0.6069 ±0.0025	0.6903 ±0.0018	0.8190 ±0.0019	0.2154 ±0.0035	0.00546 ±0.00095	0.00162 ±0.00118
Zr	59.3	5453 ±113	701 ±38	0.3184 ±0.0025	0.6169 ±0.0025	0.6963 ±0.0016	0.8229 ±0.0018	0.2175 ±0.0034	0.00432 ±0.00062	0.00196 ±0.00106
Zr	75.7	4326 ±88	557 ±30	0.3411 ±0.0027	0.6430 ±0.0028	0.7150 ±0.0018	0.8347 ±0.0019	0.2157 ±0.0044	0.00437 ±0.00051	0.00190 ±0.00138

*Production rates in 10⁻¹² cm³/g/Ma normalized to a flux density of primary protons $J_0 = 1 \text{ s}^{-1} \text{ cm}^{-2}$.

†Distance to the center in g/cm² (density iron = 7.87 g/cm³); ⁸⁵Kr is corrected for radioactive decay ($t_{1/2} = 10.7$ years). Errors at 1σ .

TABLE 2c. Measured concentrations, production rates of ⁸³Kr and Kr isotopic ratios vs. distance to the center in Y target irradiated with 1600 MeV protons in the gabbro sphere ($R = 15$ cm).

Target	r [†] (g/cm ²) (10 ⁻¹² cm ³ /g)	⁸³ Kr	P(⁸³ Kr)*	⁷⁸ Kr/ ⁸³ Kr	⁸⁰ Kr/ ⁸³ Kr	⁸¹ Kr/ ⁸³ Kr	⁸² Kr/ ⁸³ Kr	⁸⁴ Kr/ ⁸³ Kr	⁸⁵ Kr/ ⁸³ Kr	⁸⁶ Kr/ ⁸³ Kr
Y	3.3	12234 ±614	651 ±46	0.3177 ±0.0034	0.6412 ±0.0044	0.7163 ±0.0049	0.8437 ±0.0036	0.2997 ±0.0015	0.00124 ±0.00011	0.0088 ±0.00022
Y	10.2	11854 ±594	631 ±45	0.3157 ±0.0032	0.6439 ±0.0040	0.7215 ±0.0031	0.8394 ±0.0025	0.3089 ±0.0011	n.d.	0.0063 ±0.00016
Y	16.8	12089 ±605	643 ±46	0.3187 ±0.0032	0.6446 ±0.0040	0.7223 ±0.0031	0.8382 ±0.0022	0.2970 ±0.0012	0.00122 ±0.00005	0.0082 ±0.00017
Y	19.2	11167 ±560	594 ±42	0.3195 ±0.0032	0.6452 ±0.0040	0.7180 ±0.0032	0.8345 ±0.0022	0.3048 ±0.0011	0.00136 ±0.00005	0.0108 ±0.00016
Y	25.8	12174 ±611	648 ±46	0.3268 ±0.0033	0.6553 ±0.0040	0.7319 ±0.0033	0.8387 ±0.0021	0.2873 ±0.0010	0.00125 ±0.00005	0.0056 ±0.00015
Y	28.2	12437 ±624	662 ±47	0.3300 ±0.0033	0.6592 ±0.0040	0.7344 ±0.0033	0.8459 ±0.0022	0.2918 ±0.0010	0.00125 ±0.00005	0.0074 ±0.00016
Y	34.8	11591 ±581	617 ±44	0.3324 ±0.0034	0.6614 ±0.0041	0.7385 ±0.0034	0.8445 ±0.0030	0.2958 ±0.0011	0.00130 ±0.00005	0.0084 ±0.00016
Y	37.2	10669 ±536	568 ±40	0.3402 ±0.0034	0.6745 ±0.0043	0.7414 ±0.0032	0.8452 ±0.0025	0.2879 ±0.0013	0.00133 ±0.00011	0.0068 ±0.00020
Y	43.8	9848 ±492	524 ±37	0.3426 ±0.0035	0.6771 ±0.0042	0.7451 ±0.0034	0.8495 ±0.0024	0.2954 ±0.0010	0.00140 ±0.00011	0.0086 ±0.00016

*Production rates in 10⁻¹² cm³/g/Ma normalized to a flux density of primary protons $J_0 = 1 \text{ s}^{-1} \text{ cm}^{-2}$.

†Distance to the center in g cm⁻² (density gabbro = 3.0 g/cm³); ⁸⁵Kr is corrected for radioactive decay ($t_{1/2} = 10.7$ years). Errors at 1σ .
n.d. = not detected.

TABLE 3a. Measured concentrations, production rates of ^{126}Xe and Xe isotopic ratios vs. distance to the center in Ba and La targets irradiated with 1600 MeV protons in the gabbro sphere ($R = 25$ cm).

Target	r^\dagger (g/cm 2)	^{126}Xe (10^{-12} cm 3 /g)	$P(^{126}\text{Xe})^*$	$^{124}\text{Xe}/$ ^{126}Xe	$^{128}\text{Xe}/$ ^{126}Xe	$^{129}\text{Xe}/$ ^{126}Xe	$^{130}\text{Xe}/$ ^{126}Xe	$^{131}\text{Xe}/$ ^{126}Xe	$^{132}\text{Xe}/$ ^{126}Xe	$^{134}\text{Xe}/$ ^{126}Xe	$^{136}\text{Xe}/$ ^{126}Xe
Ba	6.3	1511 ± 104	361 ± 31	0.5550 ± 0.0013	1.5053 ± 0.0039	1.7350 ± 0.0078	1.2023 ± 0.0054	2.6556 ± 0.0117	1.1947 ± 0.0076	0.1083 ± 0.0013	0.01214 ± 0.00078
Ba	11.4	1634 ± 115	390 ± 34	0.5614 ± 0.0011	1.5005 ± 0.0033	1.7445 ± 0.0138	1.1929 ± 0.0040	2.6407 ± 0.0171	1.1747 ± 0.0176	0.1047 ± 0.0043	0.01020 ± 0.00190
Ba	21.9	1474 ± 104	352 ± 30	0.5616 ± 0.0014	1.4983 ± 0.0029	1.7141 ± 0.0067	1.1974 ± 0.0042	2.6150 ± 0.0130	1.1816 ± 0.0082	0.1071 ± 0.0017	0.01110 ± 0.00090
Ba	26.4	1504 ± 104	359 ± 31	0.5623 ± 0.0013	1.5000 ± 0.0033	1.7191 ± 0.0100	1.1976 ± 0.0058	2.6202 ± 0.0160	1.1761 ± 0.0100	0.1073 ± 0.0016	0.01215 ± 0.00100
Ba	36.9	1663 ± 115	397 ± 34	0.5638 ± 0.0013	1.4947 ± 0.0032	1.6979 ± 0.0070	1.1902 ± 0.0050	2.6040 ± 0.0150	1.1825 ± 0.0090	0.1079 ± 0.0017	0.01020 ± 0.00100
Ba	41.4	1563 ± 108	373 ± 32	0.5639 ± 0.0017	1.4949 ± 0.0050	1.7315 ± 0.0122	1.1909 ± 0.0067	2.6060 ± 0.0100	1.1690 ± 0.0091	0.1068 ± 0.0017	0.01010 ± 0.00100
Ba	52.2	1370 ± 97	327 ± 28	0.5655 ± 0.0020	1.4835 ± 0.0051	1.6835 ± 0.0105	1.1743 ± 0.0057	2.5130 ± 0.0200	1.1776 ± 0.0100	0.1057 ± 0.0018	0.01090 ± 0.00100
Ba	57.0	1389 ± 97	332 ± 28	0.5741 ± 0.0028	1.4718 ± 0.0061	1.7071 ± 0.0141	1.1498 ± 0.0081	2.4608 ± 0.0230	1.1140 ± 0.0149	0.1040 ± 0.0020	0.01065 ± 0.00090
Ba	67.2	1218 ± 85	291 ± 25	0.5740 ± 0.0017	1.4600 ± 0.0036	1.6632 ± 0.0098	1.1585 ± 0.0044	2.4090 ± 0.0190	1.1018 ± 0.0090	0.1012 ± 0.0018	0.01020 ± 0.00110
Ba	72.6	1129 ± 78	269 ± 23	0.5726 ± 0.0015	1.4608 ± 0.0081	1.6808 ± 0.0085	1.1716 ± 0.0068	2.4390 ± 0.0200	1.1414 ± 0.0068	0.1034 ± 0.0018	0.01200 ± 0.00120
La	25.2	1485 ± 74	355 ± 25	0.6592 ± 0.0022	1.3789 ± 0.0045	1.6125 ± 0.0084	0.6192 ± 0.0042	2.3979 ± 0.0190	0.4533 ± 0.0049	0.0136 ± 0.0006	0.00272 ± 0.00044
La	25.2	1396 ± 97	333 ± 28	0.6641 ± 0.0023	1.3826 ± 0.0047	1.6239 ± 0.0081	0.6168 ± 0.0039	2.2446 ± 0.0180	0.4560 ± 0.0049	0.0142 ± 0.0004	0.00347 ± 0.00026
La	40.2	1285 ± 85	307 ± 26	0.6651 ± 0.0014	1.3736 ± 0.0028	1.6209 ± 0.0051	0.6116 ± 0.0021	2.2177 ± 0.0090	0.4584 ± 0.0030	0.0146 ± 0.0005	0.00447 ± 0.00036
La	45.9	1274 ± 85	304 ± 25	0.6696 ± 0.0011	1.3784 ± 0.0031	1.6211 ± 0.0045	0.6128 ± 0.0021	2.2153 ± 0.0090	0.4463 ± 0.0030	0.0120 ± 0.0005	0.00197 ± 0.00041
La	60.9	1229 ± 82	293 ± 24	0.6767 ± 0.0018	1.3480 ± 0.0026	1.5598 ± 0.0050	0.5980 ± 0.0025	2.1180 ± 0.0110	0.4308 ± 0.0036	0.0101 ± 0.0006	0.00078 ± 0.00045
La	70.2	717 ± 48	171 ± 14	0.6825 ± 0.0017	1.3256 ± 0.0031	1.5281 ± 0.0099	0.5834 ± 0.0032	2.0483 ± 0.0100	0.4288 ± 0.0062	0.0095 ± 0.0006	0.00151 ± 0.00040

*Production rates in 10^{-12} cm 3 /g/Ma normalized to a flux density of primary protons $J_0 = 1$ s $^{-1}$ cm $^{-2}$.

† Distance to the center in g cm $^{-2}$ (density gabbro = 3.0 g/cm 3). Errors at 1σ .

1982) and is based on the hybrid model of pre-equilibrium reactions (Blann, 1972). Except for some experimental neutron cross sections measured by Lavielle *et al.* (1990) for the production of Kr isotopes there are no experimental cross sections for the production of krypton and Xe isotopes by neutron-induced reactions. We had to rely nearly completely

on theoretical ones for the *a priori* calculations. Also these neutron cross sections were calculated with the AREL code and completed for energies above 200 MeV by HETC calculations as discussed in detail by Leya *et al.* (2000a).

Figure 1 shows experimental production rates of ^{81}Kr and ^{83}Kr from Rb, Sr, Y, and Zr as a function of depth inside the

TABLE 3b. Measured concentrations, production rates of ^{126}Xe and Xe production rate ratios vs. distance to the center in Ba and La targets irradiated with 1600 MeV protons in the iron sphere ($R = 10$ cm).

Target	r^\dagger (g/cm 2)(10 $^{-12}$ cm 3 /g)	^{126}Xe	$P(^{126}\text{Xe})^*$	$^{124}\text{Xe}/$ ^{126}Xe	$^{128}\text{Xe}/$ ^{126}Xe	$^{129}\text{Xe}/$ ^{126}Xe	$^{130}\text{Xe}/$ ^{126}Xe	$^{131}\text{Xe}/$ ^{126}Xe	$^{132}\text{Xe}/$ ^{126}Xe	$^{134}\text{Xe}/$ ^{126}Xe	$^{136}\text{Xe}/$ ^{126}Xe
Ba	16.8	2067 ± 117	266 ± 20	0.5558 ± 0.0111	1.5045 ± 0.0212	1.8403 ± 0.0253	1.2223 ± 0.0113	2.7226 ± 0.0489	1.2942 ± 0.0335	0.1480 ± 0.0185	0.03877 ± 0.01699
Ba	27.9	2334 ± 132	300 ± 23	0.5585 ± 0.0113	1.5006 ± 0.0218	1.8435 ± 0.0259	1.2193 ± 0.0115	2.7094 ± 0.0494	1.2912 ± 0.0340	0.1497 ± 0.0187	0.03915 ± 0.01726
Ba	37.2	1968 ± 109	253 ± 19	0.5604 ± 0.0089	1.5028 ± 0.0144	1.7897 ± 0.0166	1.2191 ± 0.0070	2.6750 ± 0.0352	1.2340 ± 0.0201	0.1264 ± 0.0108	0.02226 ± 0.00990
Ba	47.7	1993 ± 112	256 ± 19	0.5658 ± 0.0107	1.4939 ± 0.0196	1.7876 ± 0.0223	1.2113 ± 0.0103	2.6364 ± 0.0441	1.2472 ± 0.0293	0.1371 ± 0.0162	0.03274 ± 0.01490
Ba	55.9	2218 ± 121	285 ± 21	0.5690 ± 0.0089	1.4851 ± 0.0137	1.7319 ± 0.0144	1.1911 ± 0.0066	2.5655 ± 0.0326	1.1964 ± 0.0177	0.1192 ± 0.0097	0.01822 ± 0.00893
Ba	68.3	1650 ± 90	212 ± 16	0.5782 ± 0.0086	1.4689 ± 0.0130	1.6730 ± 0.0155	1.1648 ± 0.0065	2.4721 ± 0.0296	1.1393 ± 0.0144	0.1108 ± 0.0071	0.01320 ± 0.00653
La	14.1	2147 ± 117	276 ± 20	0.6596 ± 0.0098	1.3658 ± 0.0116	1.6325 ± 0.0097	0.6284 ± 0.0035	2.2948 ± 0.0245	0.4809 ± 0.0101	0.0183 ± 0.0042	0.00750 ± 0.00365
La	25.7	1934 ± 106	249 ± 18	0.6659 ± 0.0093	1.3749 ± 0.0092	1.6101 ± 0.0074	0.6240 ± 0.0024	2.2739 ± 0.0234	0.4692 ± 0.0053	0.0148 ± 0.0023	0.00430 ± 0.00198
La	35.2	1844 ± 100	237 ± 17	0.6707 ± 0.0093	1.3715 ± 0.0088	1.6038 ± 0.0079	0.6246 ± 0.0019	2.2497 ± 0.0227	0.4654 ± 0.0056	0.0155 ± 0.0025	0.00508 ± 0.00209
La	45.8	1857 ± 101	239 ± 18	0.6703 ± 0.0092	1.3647 ± 0.0084	1.5964 ± 0.0069	0.6249 ± 0.0019	2.2401 ± 0.0224	0.4573 ± 0.0029	0.0127 ± 0.0010	0.00197 ± 0.00085
La	53.9	1847 ± 100	238 ± 18	0.6683 ± 0.0093	1.3513 ± 0.0086	1.5787 ± 0.0078	0.6158 ± 0.0021	2.2028 ± 0.0226	0.4531 ± 0.0045	0.0133 ± 0.0020	0.00326 ± 0.00170
La	66.3	1868 ± 101	240 ± 18	0.6858 ± 0.0096	1.3321 ± 0.0086	1.5347 ± 0.0078	0.5969 ± 0.0022	2.0917 ± 0.0213	0.4393 ± 0.0045	0.0139 ± 0.0020	0.00287 ± 0.00169

*Production rates in 10^{-12} cm 3 /g/Ma normalized to a flux density of primary protons $J_0 = 1$ s $^{-1}$ cm $^{-2}$.

† Distance to the center in g cm $^{-2}$ (density iron = 7.87 g/cm 3). Errors at 1σ .

artificial stony meteoroid ($R = 25$ cm) irradiated with 1600 MeV protons in comparison with model calculations based on *a priori* neutron data.

Overall, there is an underestimation of the measured data by the calculations. Neither the absolute values of the measured data nor their depth dependence are reproduced by the model calculations. The shown example is not a special case. Similarly poor agreements were observed for nearly all target-product-combinations and for the other irradiation experiments.

Since the experimental production rates inside the different artificial meteoroids contain information on the neutron-induced production, this information can be extracted and improved neutron cross sections can be obtained provided that the proton-induced production can be reliably calculated and subtracted from the measured production rates. On the basis of the available thin-target cross sections for proton-induced production of Kr and Xe isotopes this is possible and the

excitation functions of the neutron-induced reactions can be derived by least-squares methods starting with theoretical neutron excitation functions as guess functions (Leya and Michel, 1997). To this end, the neutron excitation functions used in the *a priori* calculations were adjusted by a least-squares fit using the code STAY'SL (Perey, 1977) in a form modified by Matzke (1979) to fit simultaneously all available data from the simulation experiments. Since spectra of the secondary neutrons in the artificial meteoroids depend on the primary proton energies, on the chemical composition of the meteorite mock-ups, and on depth and size of the artificial meteoroids, the procedure allows for an energy-dependent fit. This adjustment is done in such a way that existing experimental data or evaluated (experimental) cross sections, which occasionally exist up to 30 MeV, are not changed by the fit. Only those parts are subject to adjustment for which only theoretical data are available.

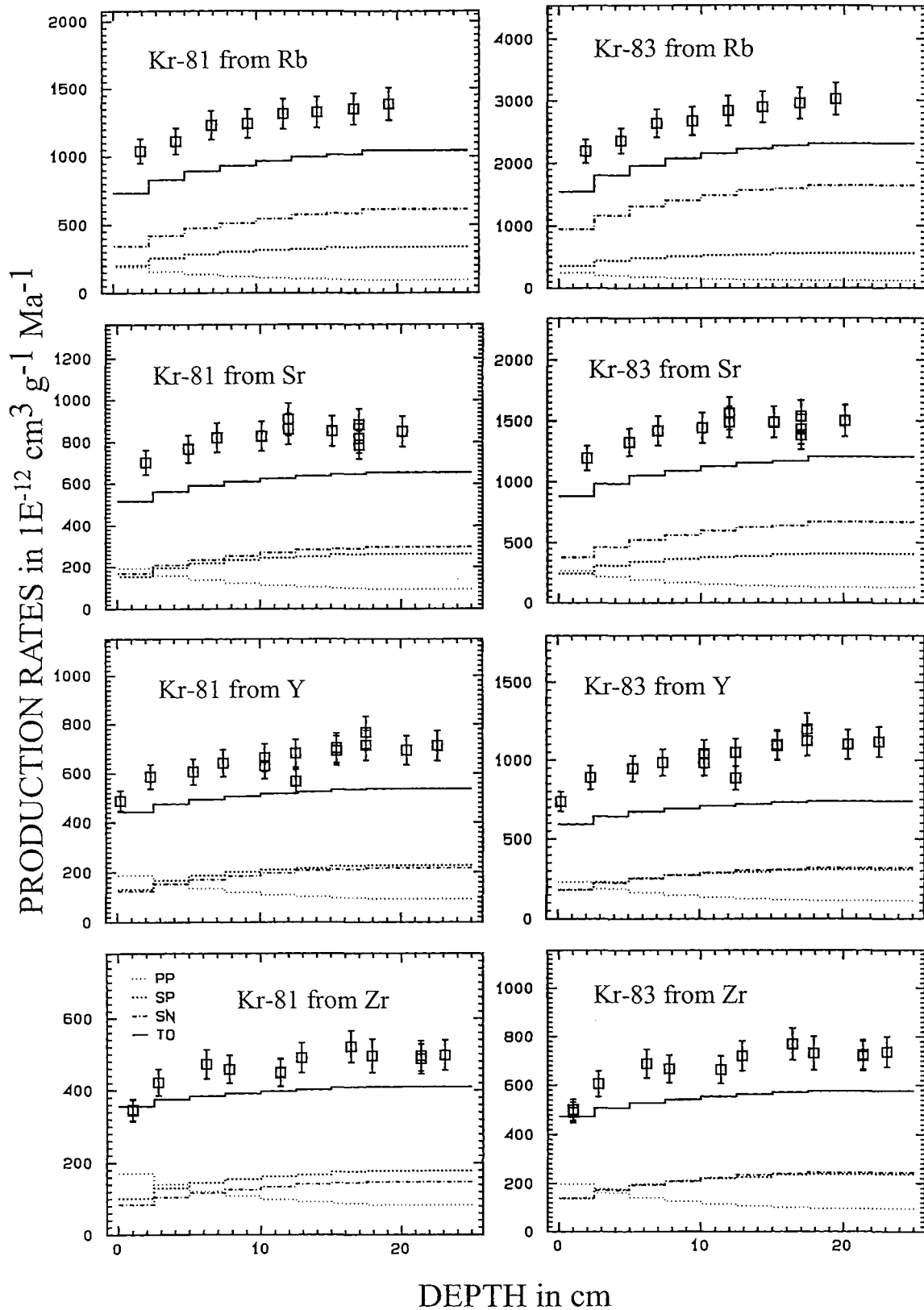


FIG. 1. Experimental production rates and the results of *a priori* model calculations of the production of ^{81}Kr and ^{83}Kr from rubidium, strontium, yttrium and zirconium in the gabbro sphere irradiated with 1600 MeV protons at LNS. Calculated production rates are code as PP for primary protons, SP for secondary protons, SN for secondary neutrons and TO for the total production.

For the Kr isotopes the thick-target production rates of the two 1600 MeV experiments with the 25 cm gabbro and the 10 cm iron sphere were used as the basis for unfolding procedure. For the Xe isotopes only the production rates for the 25 cm gabbro sphere irradiated with 1600 MeV protons were used in the unfolding.

Figures 2 and 3 show the excitation functions for the production of krypton isotopes by proton- and neutron-induced reactions from Rb, Sr, Y, and Zr used in the *a posteriori* model calculations.

Figures 4 and 5 show the production rates of ^{78}Kr from Zr and ^{84}Kr from Rb as a function of depth inside the artificial meteoroids together with the results of *a posteriori* model calculations which make use of the adjusted neutron excitation functions. The contributions of primary protons (pp), secondary protons (sp) and secondary neutrons (sn) are distinguished. Figure 4 gives an example of relatively bad agreement between experimental data and *a posteriori* model calculations; Fig. 5 is a more typical example. Mostly, there is excellent agreement between experimental and calculated production rates as indicated by Figs. 5 and 8. Both absolute values of the data and their depth dependence are usually described by the model calculations within the limits of experimental uncertainties. Exceptions are the very neutron-rich and neutron-poor isotopes for which the neutron-induced cross sections are not as well known as for the isotopes close to the valley of stability.

Using this method, a complete set of adjusted neutron excitation functions was calculated for the production of Kr and Xe isotopes from each of the target elements. Figures 6 and 7 give the proton and *a posteriori* neutron cross sections for the production of Xe isotopes from Ba and La, respectively.

As pointed out elsewhere (Michel and Neumann, 1998), the distinction between proton and neutron excitation functions is essential and an assumption of equal proton and neutron cross sections is almost never justified. The differences between proton and neutron excitation functions can be striking (Figs. 2, 3, 6, and 7). They are due to physical reasons and not artifacts of the adjustment procedure for energies up to a few hundred million electronvolts. The production rates in our experiments are not sensitive to neutrons with energies above a few hundred million electronvolts because of the roughly $1/E$ dependence of the neutron spectra.

Similarly good agreement between measured and *a posteriori* calculated data is observed for nearly all target-product-combinations except for some Kr isotopes from Y and for Xe isotopes from the 600 MeV simulation experiment as discussed below.

DISCUSSION

Measurements and model calculations of ^{83}Kr production rates for the target element Rb, irradiated inside the different spheres are presented on Fig. 8 vs. the distance to the center

expressed in g cm^{-2} . Strontium, Y and Zr were irradiated with 1600 MeV incident protons at SATURNE in both gabbro and iron spheres. Rubidium was also irradiated at SATURNE but in the gabbro sphere only. For the experiment performed at CERN, only Y was irradiated with 600 MeV incident protons inside a gabbro sphere. The investigated samples taken in the same core come from locations symmetric relative to the center. Considering the same target element, no systematic shifts are visible in the production profiles indicating the spheres were irradiated isotropically.

Bulk Chemistry or Matrix Effects for the Krypton-83 Production

All depth profiles show similar trends. Starting from the surface we observe a steep increase followed by an almost flat shape up to the center. Relative to the production in the center, the total increase is $\sim 30\%$ for all investigated target elements. At the center of both the gabbro (empty symbols) and the iron (black symbols) spheres, the ^{83}Kr production is $\sim 4.1\times$ larger in Rb, $2.6\times$ larger in Sr, and $2.0\times$ larger in Y than that measured in Zr targets. These factors are mainly due to the increase of production cross sections when the mass difference between target and product decreases.

When expressed in g cm^{-2} , the relative sizes of the two spheres irradiated at SATURNE are quite comparable. The radius of the gabbro sphere corresponds to 75 g cm^{-2} and that of the iron sphere to 78.7 g cm^{-2} . Because the irradiation conditions are similar for the two experiments after normalization to the same proton fluence, we can evaluate the specific role played by the bulk chemistry in the Kr production. Such effects of bulk chemistry on the production rates of Ne isotopes were first observed by Begemann and Schultz (1988) and strongly affect, for instance, the depth and size indicator $^{22}\text{Ne}/^{21}\text{Ne}$. This so-called matrix effect in case of Ne isotopes is well understood by model calculations (Michel *et al.*, 1990; Masarik and Reedy, 1994). Considering the same target element Sr, Y, or Zr, the measured ^{83}Kr production rates appear to be very close in the two spheres although these bodies have quite different chemical compositions. If we compare Kr isotopic ratios in the two 1600 MeV experiments (see below) we concluded that ratios are not very sensitive to the chemistry. That demonstrates that the development of the spectrum of primary and secondary particles vs. depth, when expressed in g cm^{-2} , is not sensitive to the chemical composition of the spheres. Generally, the matrix effect appears to affect the Kr (and Xe) production not much as exhibited by the differences in both experimental and calculated production rates.

In contrast, for the experiment at CERN, "gabbro 600 MeV", the measured ^{83}Kr production is lower by a factor of 2 than for the other experiments. This difference is mainly due to the lower energy of the incident protons (600 MeV compared to 1600 MeV), that causes lower neutron multiplicities and limits the development of the secondary particle flux inside the sphere.

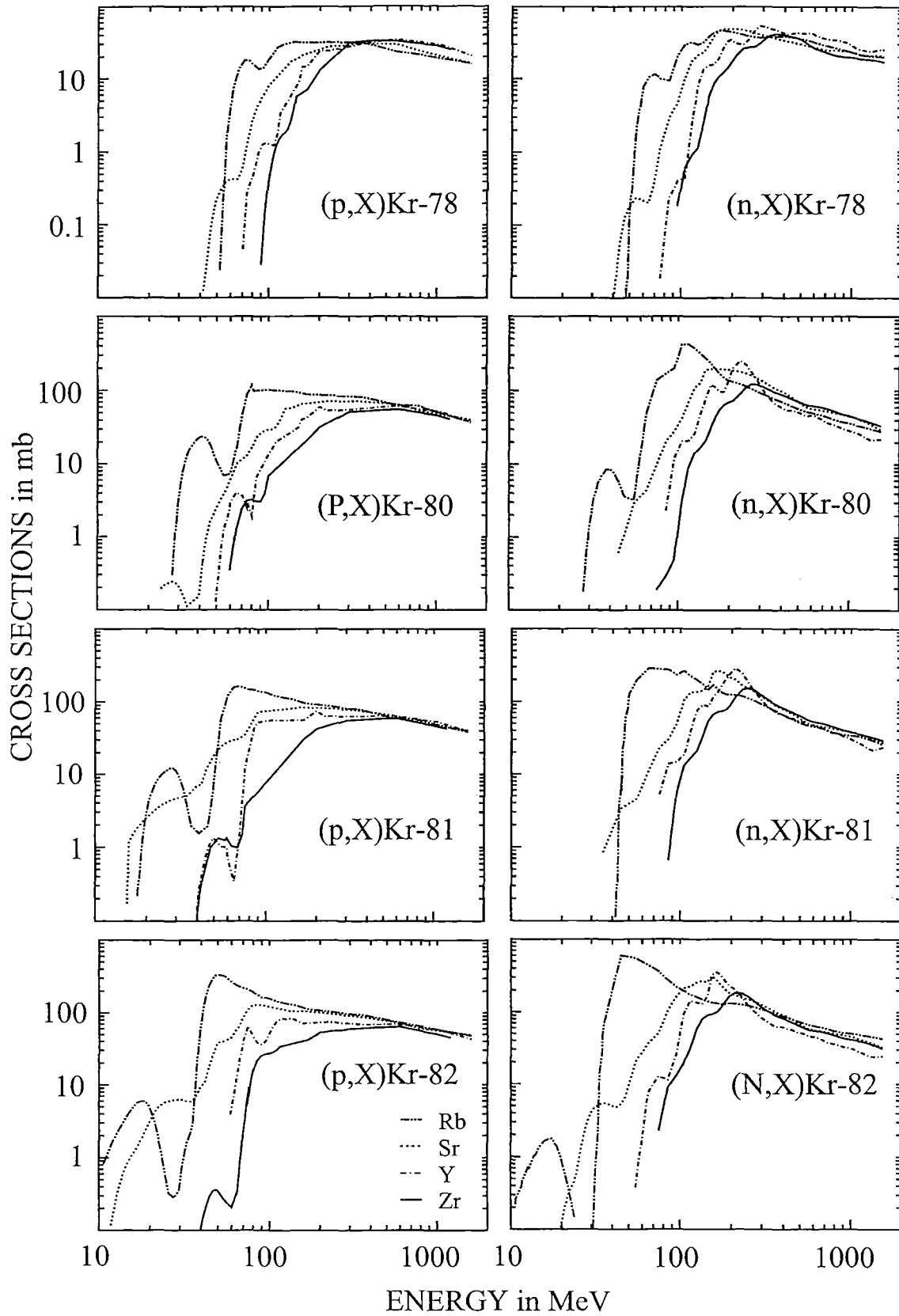


FIG. 2. Excitation functions for the proton- and neutron-induced production of ^{78}Kr , ^{80}Kr , ^{81}Kr , and ^{82}Kr from rubidium, strontium, yttrium and zirconium used for the *a posteriori* model calculations.

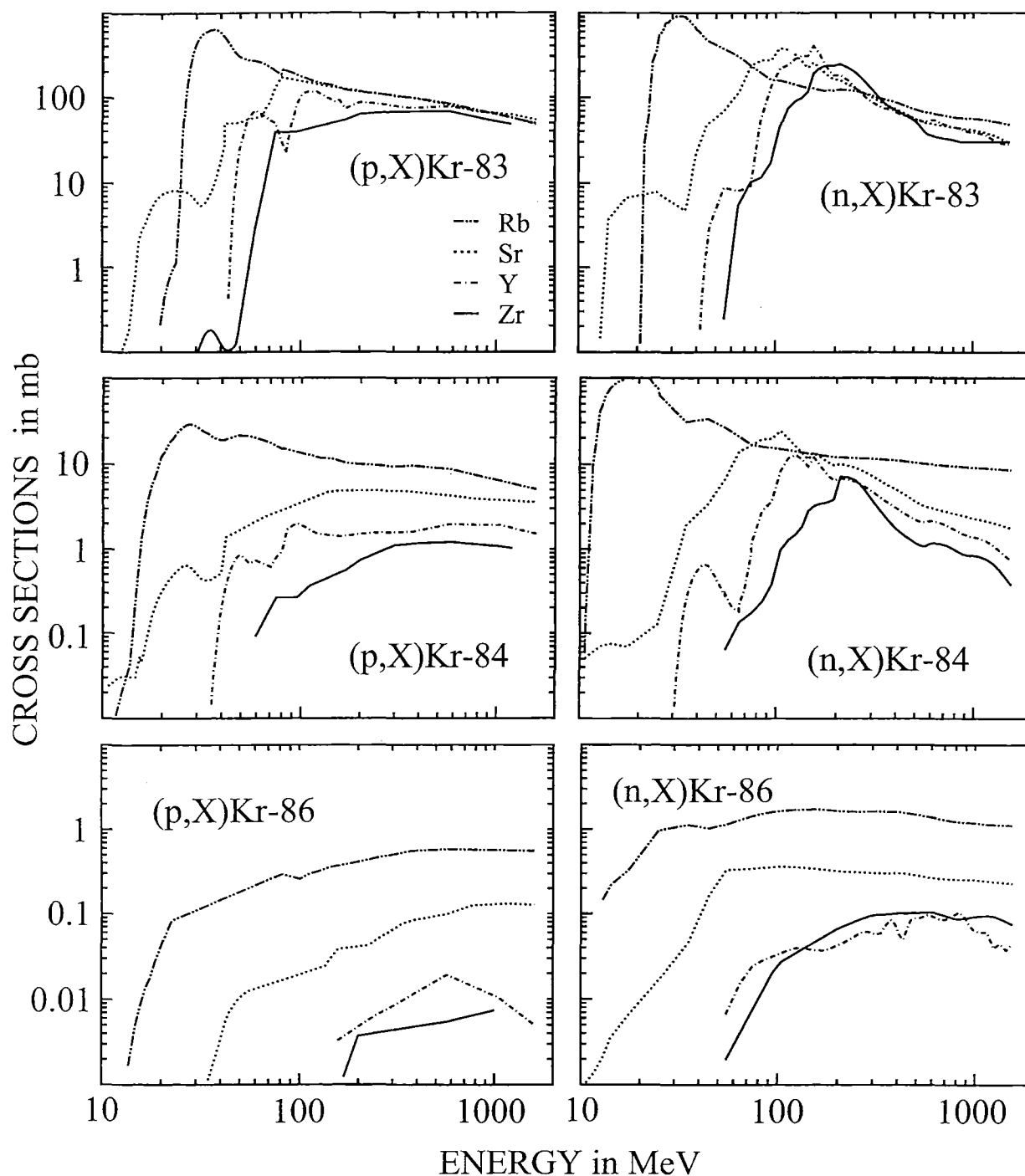


FIG. 3. Excitation functions for the proton- and neutron-induced production of ^{83}Kr , ^{84}Kr , and ^{86}Kr from rubidium, strontium, yttrium and zirconium used for the *a posteriori* model calculations.

Calculated Krypton Production Rates in Gabbro and Iron Spheres and Comparison with Measurements

As shown in Fig. 8, calculated production rates of ^{83}Kr agree well with the measured depth profiles for the two SATURNE experiments. For all investigated target elements, the observed increase of the production rates from the surface

to the center of the spheres is reproduced within experimental uncertainties except for locations very close to the surface. In this case, calculations overestimate the rates obtained from measurements by 10 to 20%. For the experiment performed at CERN at 600 MeV, calculated production rates of ^{83}Kr from Y are systematically higher by 20% than the measured one but causes of this discrepancy could not be identified. Comparing

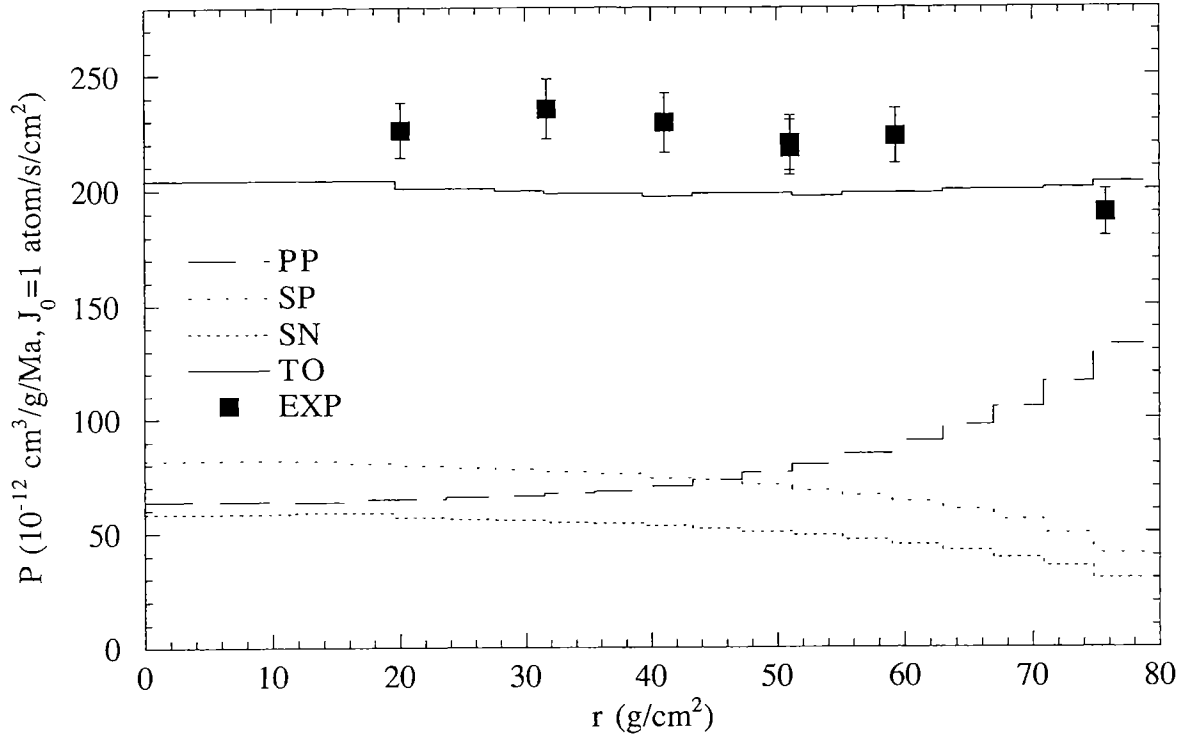


FIG. 4. Experimental and calculated ^{78}Kr production rates from zirconium in units of $10^{-12} \text{ cm}^3 \text{ g}^{-1} \text{ Ma}^{-1}$ (normalised to $J_0 = 1 \text{ s}^{-1} \text{ cm}^{-2}$) in the iron sphere vs. the distance from its centre in units of g cm^{-2} . The total calculated production and the contributions of primary and secondary protons and of secondary neutrons are shown. Calculated production rates are code as PP for primary protons, SP for secondary protons, SN for secondary neutrons and TO for the total production.

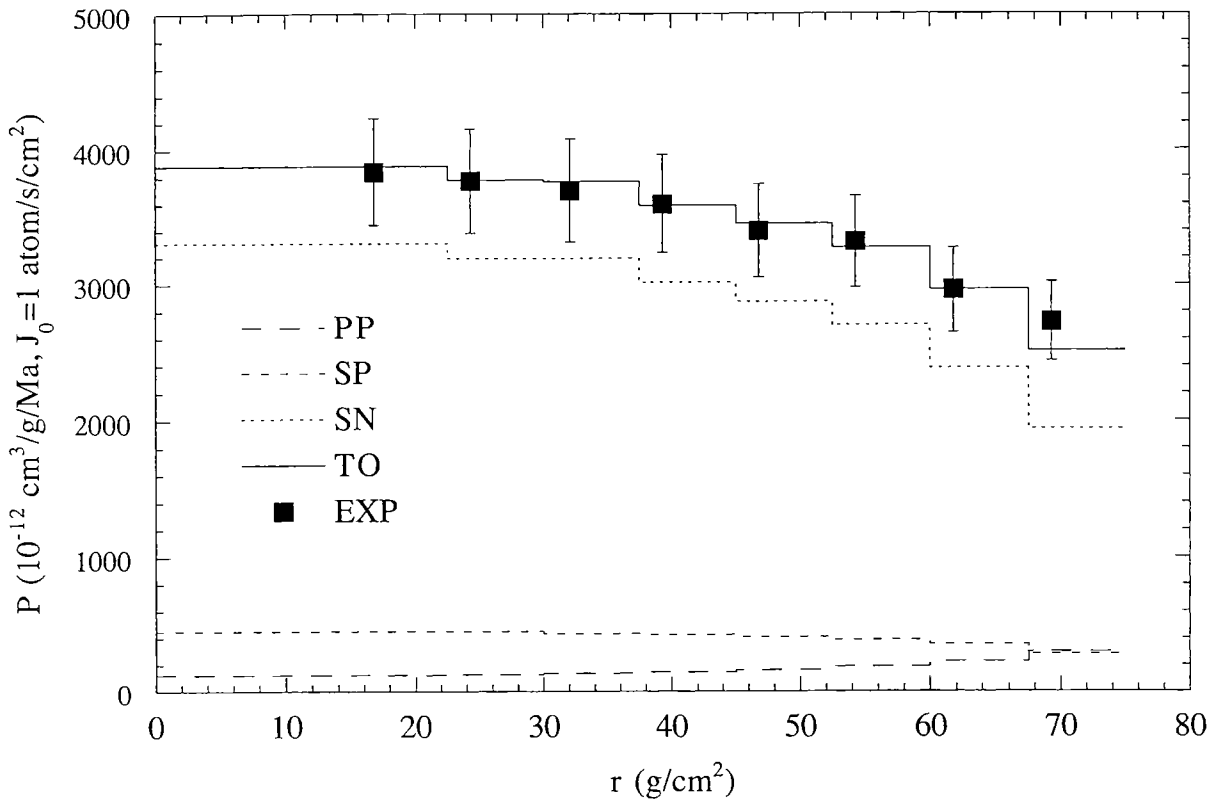


FIG. 5. Experimental and calculated ^{84}Kr production rates from rubidium in units of $10^{-12} \text{ cm}^3 \text{ g}^{-1} \text{ Ma}^{-1}$ (normalised to $J_0 = 1 \text{ s}^{-1} \text{ cm}^{-2}$) in the gabbro sphere irradiated with 1600 MeV protons at LNS vs. the distance from the center in units of g cm^{-2} . The total calculated production and the contributions of primary and secondary protons and of secondary neutrons is shown. Calculated production rates are code as PP for primary protons, SP for secondary protons, SN for secondary neutrons and TO for the total production.

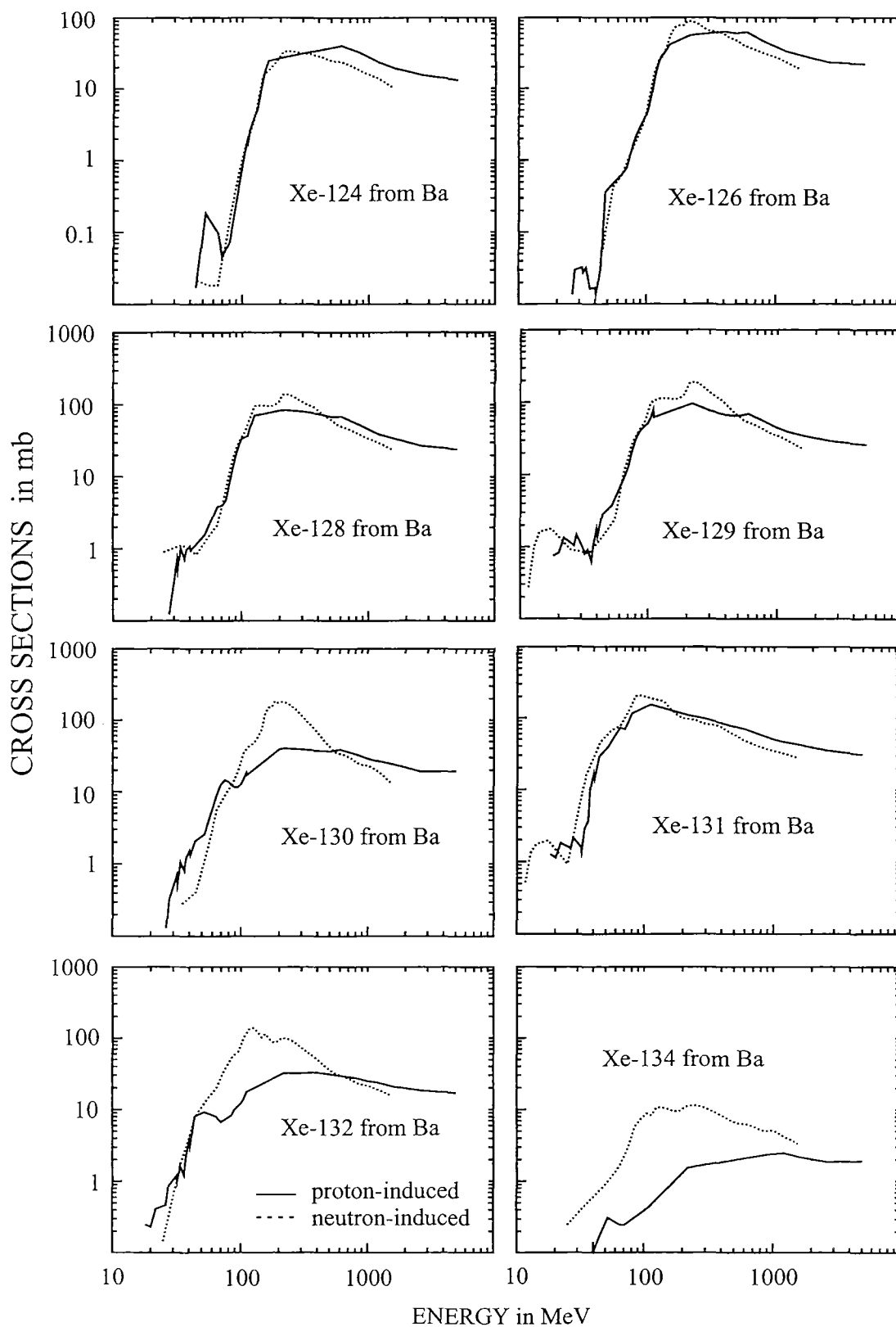


FIG. 6. Excitation functions for the proton- and neutron-induced production of xenon isotopes from barium used for the *a posteriori* model calculations.

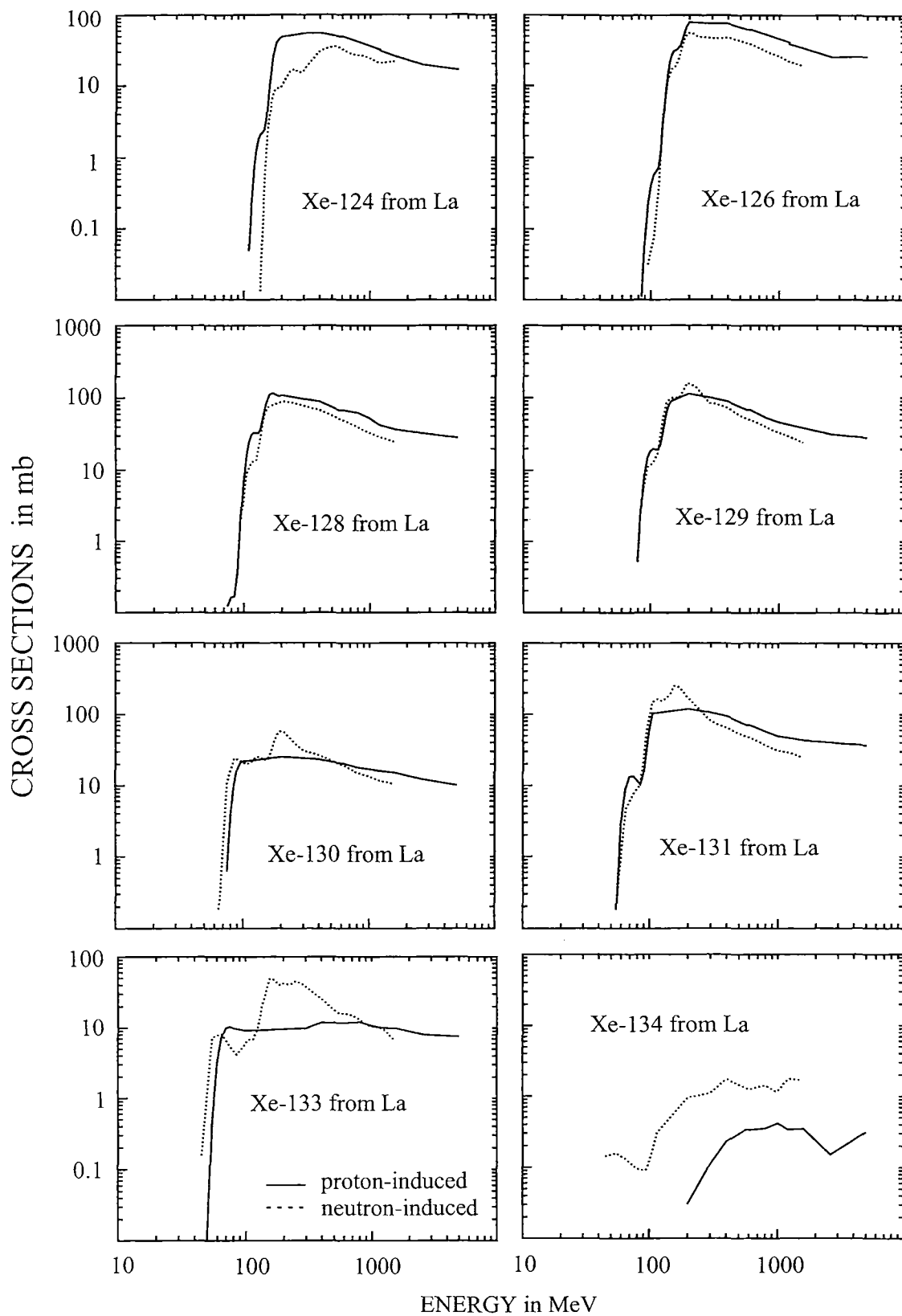


FIG. 7. Excitation functions for the proton- and neutron-induced production of xenon isotopes from lanthanum used for the *a posteriori* model calculations.

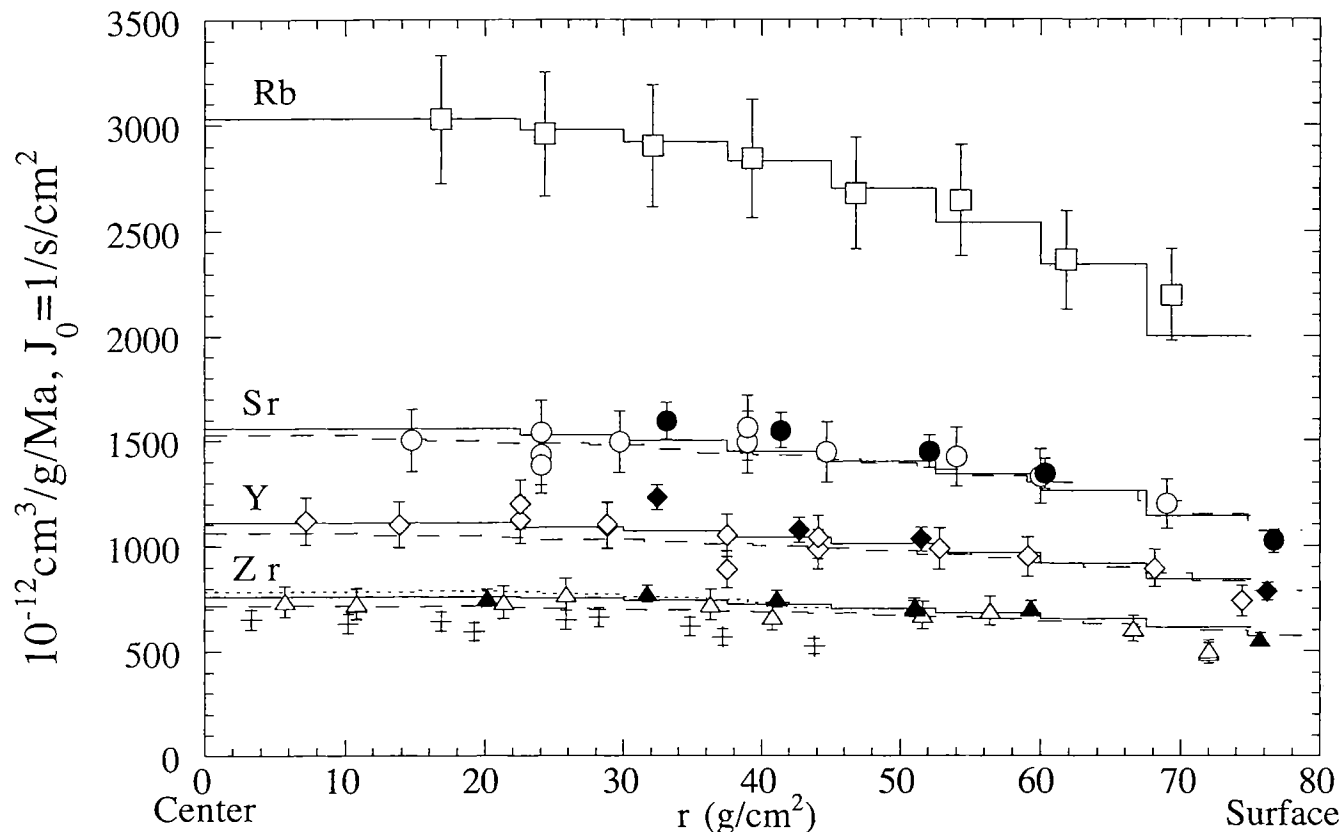


FIG. 8. Experimental and calculated ^{83}Kr production rates are presented in units of $10^{-12} \text{ cm}^3 \text{ g}^{-1} \text{ Ma}^{-1}$ (normalized to $J_0 = 1 \text{ s}^{-1} \text{ cm}^{-2}$) for different targets and spheres vs. the distance from the center in units of g cm^{-2} . Experiments with 1600 MeV protons are reported using empty symbols (measurements) and solid lines (calculations) in case of the gabbro sphere and filled symbols and dashed lines in case of the iron sphere. Crosses and dotted lines are used for the experimental results and the model calculations, respectively, for the experiment with a gabbro sphere ($R = 25 \text{ cm}$) irradiated with 600 MeV protons at CERN. Note that all calculated production rates are from *a posteriori* calculations unless otherwise stated.

the production in the two spheres at SATURNE, calculations lead to a possible small matrix effect, in agreement with measurements. Calculated production rates are found to be only 3 to 6% larger in gabbro (full lines) compared to iron (dashed lines) depending on the considered target element.

In Figs. 4 and 5, we present calculated and measured production rates, respectively, for ^{78}Kr from Zr in the iron sphere and of ^{84}Kr from Rb in the gabbro sphere. These plots illustrate two examples of Kr production involving quite different secondary particle fluxes. Dashed curves show calculated productions due to the primary protons, and due to the secondary protons and neutrons. In both cases, the calculated total contributions shown by the solid curves are in good agreement with measurements reported by the black squares. For ^{78}Kr , except near the surface where primary protons dominate, each type of incident particles supplies about one-third of the total, leading to a rather flat depth profile. On the other hand, the ^{84}Kr profile rapidly increases from the surface to the center with a dominant contribution from the secondary neutrons. In all cases, the contribution of secondary neutrons to the total Kr production is always important as shown on Fig. 9 for all Kr isotopes. For the two experiments at SATURNE,

it ranges from 25% for ^{78}Kr from Zr in the iron target to 83% for ^{84}Kr from Rb in the gabbro target. That underlines the importance of the determination of the neutron-induced production that requires reliable neutron-induced cross sections. The general agreement found between measurements and calculations for the different experiments validates most of the neutron-induced excitation functions derived from this work following the procedure described above.

Production ratios for all other Kr isotopes are presented relative to ^{83}Kr for the experiments performed at SATURNE in Fig. 10 for gabbro and in Fig. 11 for iron. Results for the experiment at 600 MeV done at CERN are shown by Fig. 12a,b. Similar to the absolute ^{83}Kr production, the measured production ratios exhibit, for a given target element, almost the same profiles in the two spheres irradiated at SATURNE, indicating that the chemistry of the irradiated body does not much affect the Kr production from the target elements, Sr, Y, and Zr. For all Kr isotopes, experimental production rates are consistent in the two spheres to within 4%.

The ratios $^{78}\text{Kr}/^{83}\text{Kr}$, $^{80}\text{Kr}/^{83}\text{Kr}$, $^{81}\text{Kr}/^{83}\text{Kr}$, and $^{82}\text{Kr}/^{83}\text{Kr}$ show similar trends in all targets: a decrease from the surface to the center. The ratio $^{78}\text{Kr}/^{83}\text{Kr}$ has the most important variations

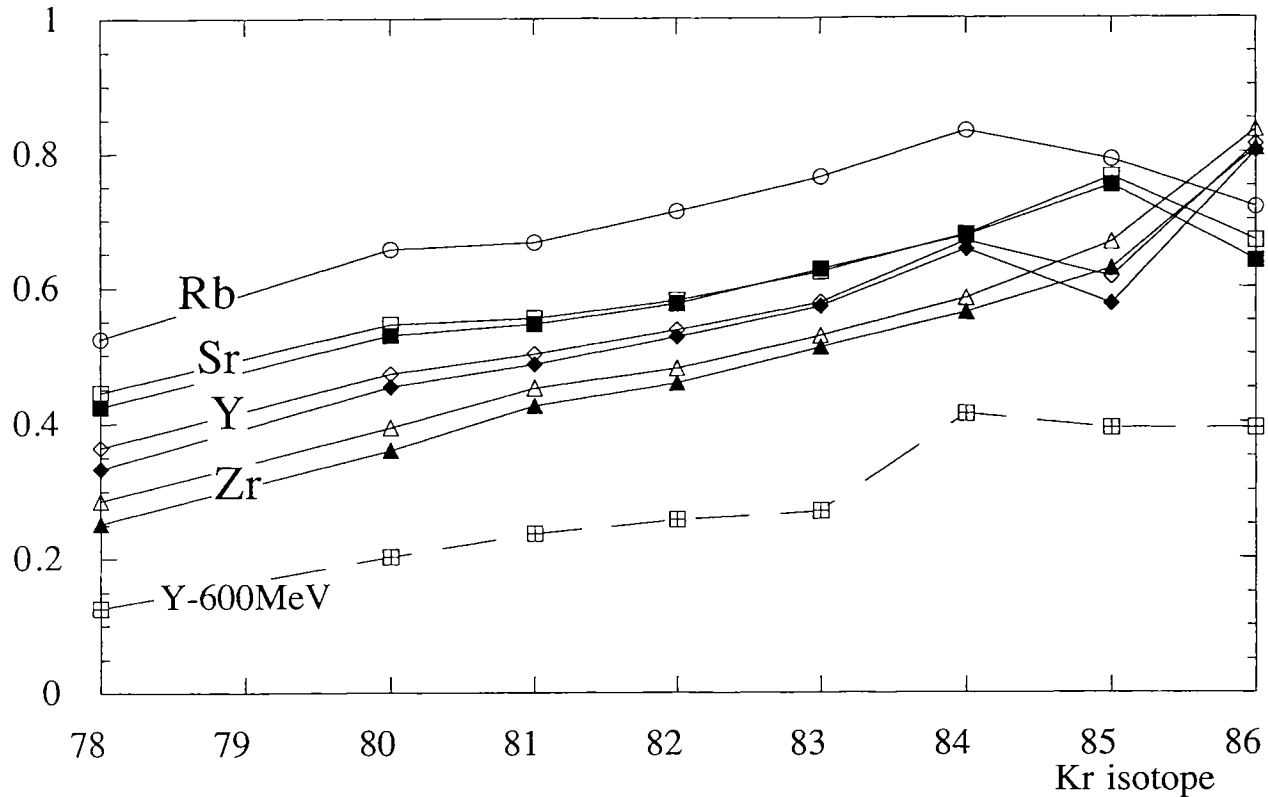


FIG. 9. Calculated fraction of the contribution of secondary neutrons relative to the total production of the different Kr isotopes and target elements in the gabbro and iron spheres irradiated with 1600 MeV protons at LNS. Filled and empty symbols are for iron and gabbro spheres. Crossed square symbols are 600 MeV CERN sphere.

with ~10% decrease for all the target elements. This is the reason why this ratio represents the best choice among Kr isotope ratios for monitoring the shielding depth of the samples in meteorites. The total variations are about 6, 4 and 2%, respectively, for $^{80}\text{Kr}/^{83}\text{Kr}$, $^{81}\text{Kr}/^{83}\text{Kr}$ and $^{82}\text{Kr}/^{83}\text{Kr}$ in all the targets. On the other hand, depth profiles concerning neutron-rich Kr isotopes are rather flat or even increase from the surface to the center of the spheres such as $^{84}\text{Kr}/^{83}\text{Kr}$ in Rb.

A second clear effect is related to the mass of the target elements. Again, neutron-poor and neutron-rich isotopes show distinct trends. At a given depth, the production ratios $^{78}\text{Kr}/^{83}\text{Kr}$, $^{80}\text{Kr}/^{83}\text{Kr}$, $^{81}\text{Kr}/^{83}\text{Kr}$, and $^{82}\text{Kr}/^{83}\text{Kr}$ clearly increase with the mass of the target elements. The production ratio $^{78}\text{Kr}/^{83}\text{Kr}$ is 3× larger in Zr than in Rb. Relative to ^{78}Kr which is a neutron-poor isotope, ^{83}Kr is more efficiently produced by low-energy particles in Rb than in Zr in which reaction thresholds are much higher, leading in Rb to a lower $^{78}\text{Kr}/^{83}\text{Kr}$ ratio. For $^{84}\text{Kr}/^{83}\text{Kr}$, $^{85}\text{Kr}/^{83}\text{Kr}$ and $^{86}\text{Kr}/^{83}\text{Kr}$ the trend is completely different. The production ratio $^{84}\text{Kr}/^{83}\text{Kr}$ is 6× larger in Rb than in Zr, reflecting the important role played by secondary neutrons in the production of neutron-rich isotopes, such as ^{84}Kr , when the mass difference between target elements and products is small.

In Fig. 12b, $^{86}\text{Kr}/^{83}\text{Kr}$ does not agree with the calculations. Cross section of ^{86}Kr in Y is not very well known (Gilbert *et al.*, 1998) but in gabbro and iron experiments there is a good

agreement with calculations (Figs. 10 and 11). The discrepancy is certainly due to bad air corrections for ^{86}Kr (see comments in section "Target Blanks").

The excellent match between measurements and calculations validates the ability of the interaction model to reproduce the particle fluxes produced in the spheres, leading to realistic Kr production rates when reliable excitation functions are available as is the case for the four investigated target elements, Rb, Sr, Y, and Zr (Gilbert *et al.*, 1998). Of course, all production depth profiles depend on the size of the irradiated object and on the energy of the incident particles. The influence of these parameters on production will be investigated in a future paper along the line of model calculations for cosmogenic radionuclides in meteorites by Leya *et al.* (2000b) and by Michel and Neumann (1998), considering the case of meteoroids of different sizes irradiated in space by a realistic flux of cosmic-ray particles.

Xenon in Gabbro and Iron Spheres Irradiated at SATURNE

Xenon production in Ba and La shows similar depth profiles to that of Kr, namely an increase from the surface to the center and a flat shape near the center, as illustrated by Fig. 13. In this figure, production profiles of ^{126}Xe are presented in La and Ba in the two spheres made of gabbro and of iron vs. the

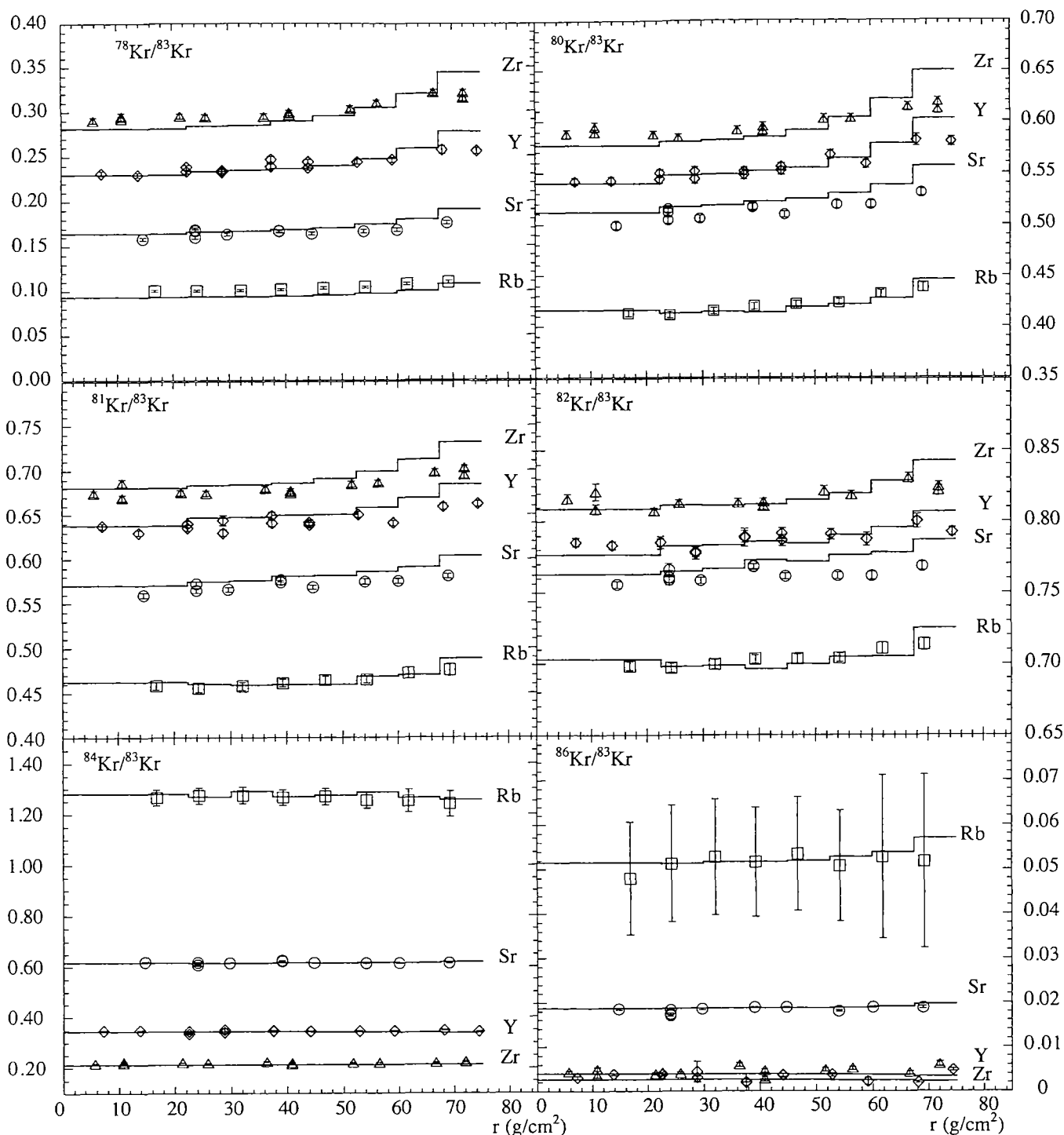


FIG. 10. Experimental and calculated Kr production rate ratios in the gabbro sphere ($R = 25$ cm) irradiated with 1600 MeV protons at LNS vs. the distance from the centre in units of g cm^{-2} .

depth expressed in g cm^{-2} . As for Kr, no structures are visible even though, for the same profile, analyzed samples come from opposite locations relative to the center. For the two spheres, the ^{126}Xe production from Ba at the center is a few percent higher than that from La. On the other hand, it appears to be higher by $\sim 30\%$ in gabbro than in iron. Model calculations

also shown in the figure correctly predict the small production excess in Ba relative to La in both spheres but do not reproduce the difference found in the absolute production measured in the gabbro and in the iron. However, such a discrepancy could be related to the knowledge of cross sections that could not be precise enough for these two elements.

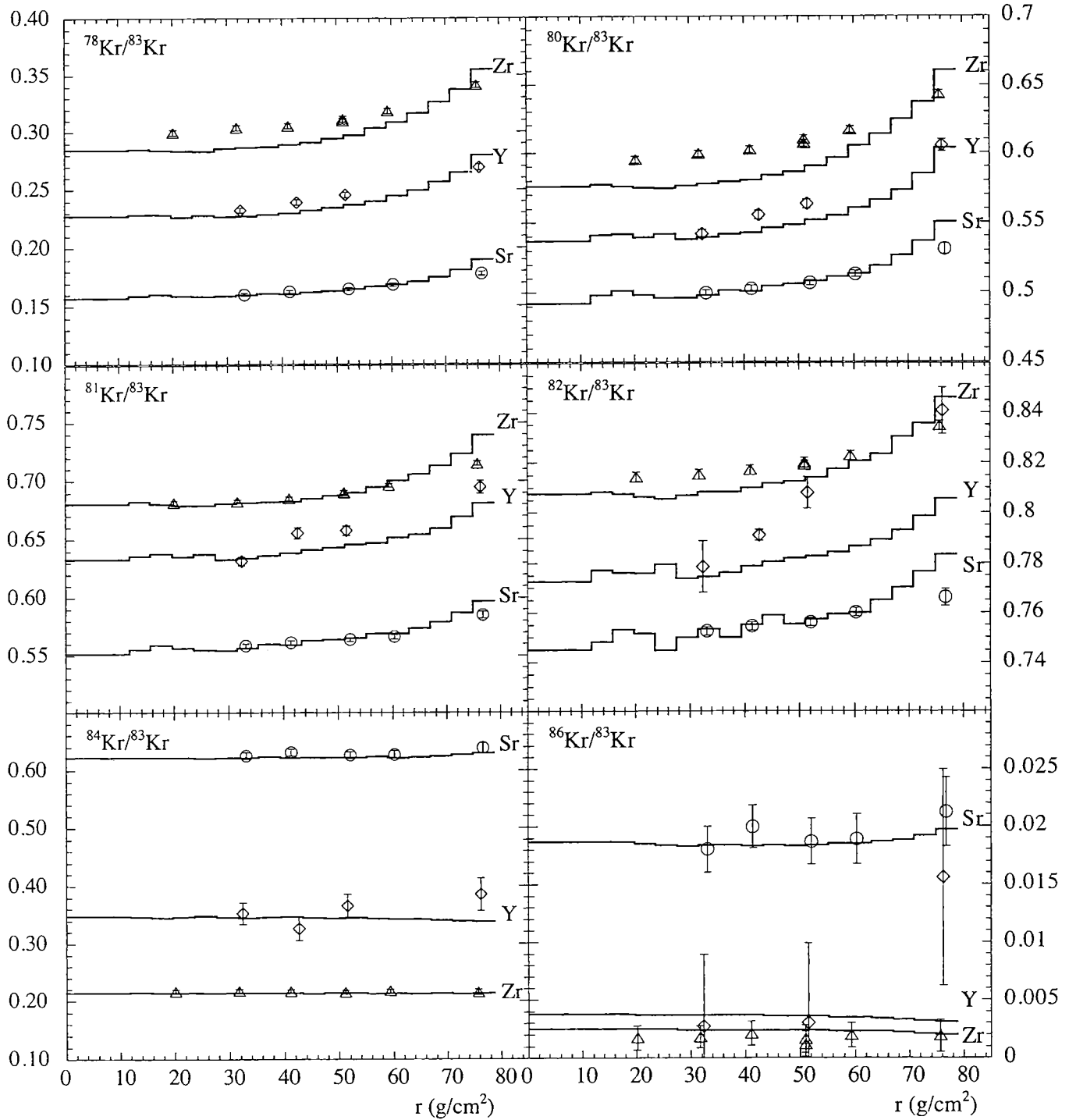


FIG. 11. Experimental and calculated Kr production rate ratios in the thick iron sphere ($R = 10$ cm) irradiated with 1600 MeV protons at LNS vs. the distance from the centre in units of g/cm^2 .

Figure 14 presents the different contributions (primary protons, secondary protons and neutrons) to the total production of ^{126}Xe from Ba vs. the depth (g/cm^2) in the two spheres. For both spheres, the ^{126}Xe production is essentially induced by secondary particles and $\sim 50\%$ is due to neutrons.

In Fig. 15, we report experimental and calculated production ratios of the Xe isotopes relative to ^{126}Xe from Ba and La targets for the two irradiation experiments performed at SATURNE. For the ratio $^{124}\text{Xe}/^{126}\text{Xe}$ we observe a decrease of 10% from the surface to the center for the two investigated

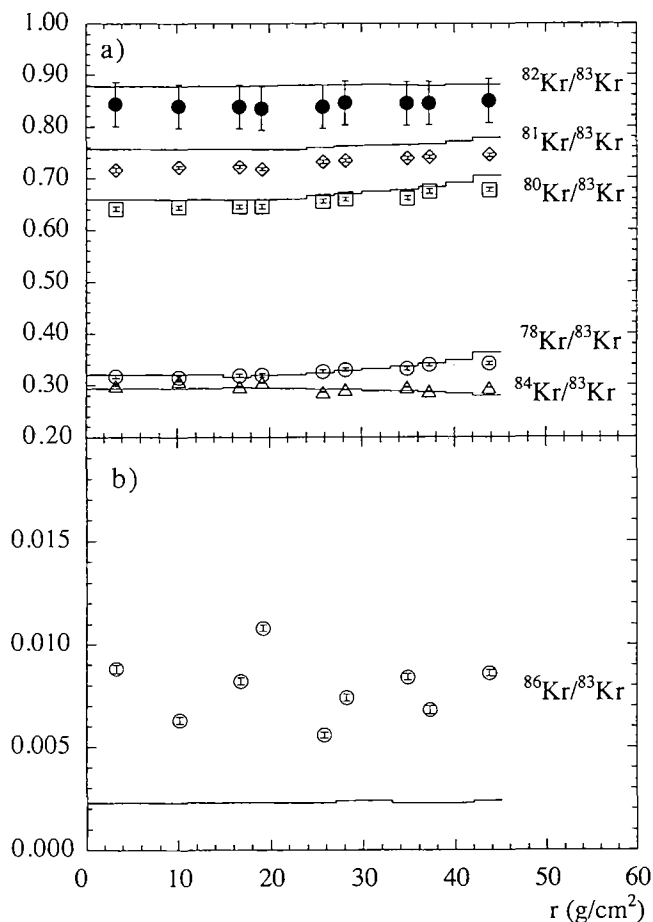


FIG. 12. Experimental and calculated Kr production rate ratios in the thick gabbro sphere ($R = 25$ cm) irradiated with 600 MeV protons at CERN vs. the distance from the centre in units of g cm^{-2} .

targets. The production ratio is 20% higher in La compared to Ba. On the other hand, for all other Xe production ratios, depth profiles are increasing from the surface to the center. Measured ratios in Ba are systematically larger than in La. Most experimental depth profiles are reproduced by calculations within a few percent.

Also contrary to Kr, experimental production ratios for Ba are slightly higher in the iron sphere than in the gabbro sphere; therefore, there are no clear trends for La. This matrix effect found for neutron-rich Xe isotopes is also well reproduced by calculations in Ba for the ratio $^{131}\text{Xe}/^{126}\text{Xe}$.

SUMMARY

We report the systematic study of Kr and Xe production in a set of simulation experiments of galactic cosmic-ray proton interactions with stony and iron meteorites. Two spheres made of gabbro and iron of 25 and 10 cm radius and containing more than 50 thin targets of Rb, Sr, Y, and Zr regularly distributed in perpendicular cores were isotropically irradiated at the SATURNE cyclotron with 1600 MeV protons. Concentrations of Kr and Xe isotopes were measured in the targets by

conventional mass spectrometer supplying precise production rate depth profiles. New Kr results from an experiment previously performed at CERN with a gabbro sphere of 15 cm radius isotropically irradiated by 600 MeV protons are also presented.

By using a physical model, theoretical production rates are calculated by folding depth-dependent spectra of primary and secondary protons and secondary neutrons with the excitation functions of the involved nuclear reactions. The comparison of the model calculations with experimental data in the thick target experiments performed at LNS and at CERN allowed adjustments of the poorly known excitation functions induced by neutrons. For the two experiments at SATURNE, general excellent agreement is obtained between experimental and calculated production rates for most Kr and Xe isotopes in all investigated target elements. Only Xe production in Ba in the gabbro is underestimated in the calculations by $\sim 25\%$. This work validates thin-target model calculations of cosmogenic nuclide production rates for determining interactions of galactic cosmic-ray protons with stony and iron meteorites in space as well as with lunar samples.

Acknowledgements—The experiments described here were a joint effort of eight European laboratories from Bordeaux, Hannover, Jülich, Köln, Mainz, Paris, and Zürich. The authors are grateful to the Laboratoire National Saturne/Saclay for performing the irradiations and to the staff of the laboratory for the kind cooperation and for essential support. This work was supported by the Deutsche Forschungsgemeinschaft, the Swiss National Science Foundation, CNRS, INSU (Programme National de Planétologie) and the University of Bordeaux I. Financial assistance towards the cost of the irradiations coming from Max-Planck-Gesellschaft *via* F. Begemann is also gratefully acknowledged. The irradiation apparatus was built and operated by personnel of the Abteilung Nuklearchemie, Universität zu Köln. We acknowledge essential contributions by R. Berndt, M. Kreikler, and U. Otto. Useful suggestions for improvements in the text were made by D. Smith.

Editorial handling: E. K. Zinner

REFERENCES

- ARMSTRONG T. W. AND CHANDLER K. C. (1972) HETC—A high-energy transport code. *Nucl. Sci. Eng.* **49**, 110.
- BEGEMANN F. AND SCHULTZ L. (1988) The influence of bulk composition on the production rate of cosmogenic nuclides in meteorites (abstract). *Lunar Planet. Sci.* **19**, 51–52.
- BLANN M. (1972) Hybrid model for pre-equilibrium decay in nuclear reactions. *Phys. Rev. Lett.* **27**, 337–340.
- BLANN M. AND BISPLINGHOFF J. (1982) *Computer code Alice Livermore 82*. UCID-19614.
- CLOTH P., FILGES D., NEEF R. D., STERZENBACH G., REUL CH., ARMSTRONG T. W., COLBORN B. L., ANDERS B. AND BRÜCKMANN H. (1988) *HERMES—High-Energy Radiation Monte-Carlo Elaborate System*. JUEL-2203, KFA Jülich, Jülich, Germany. 172 pp.
- DRAGOVITSCH P. (1987) Über die produktion kosmogener nuklide in meteoroiden—Simulationsexperimente und modellrechnungen. Ph.D. thesis, University of Cologne, Germany. 261 pp.
- EMMETT M. B. (1975) *The MORSE Monte-Carlo Radiation Code System*. ORNL-4972, Oak Ridge Natl. Lab., Oak Ridge, Tennessee, USA.

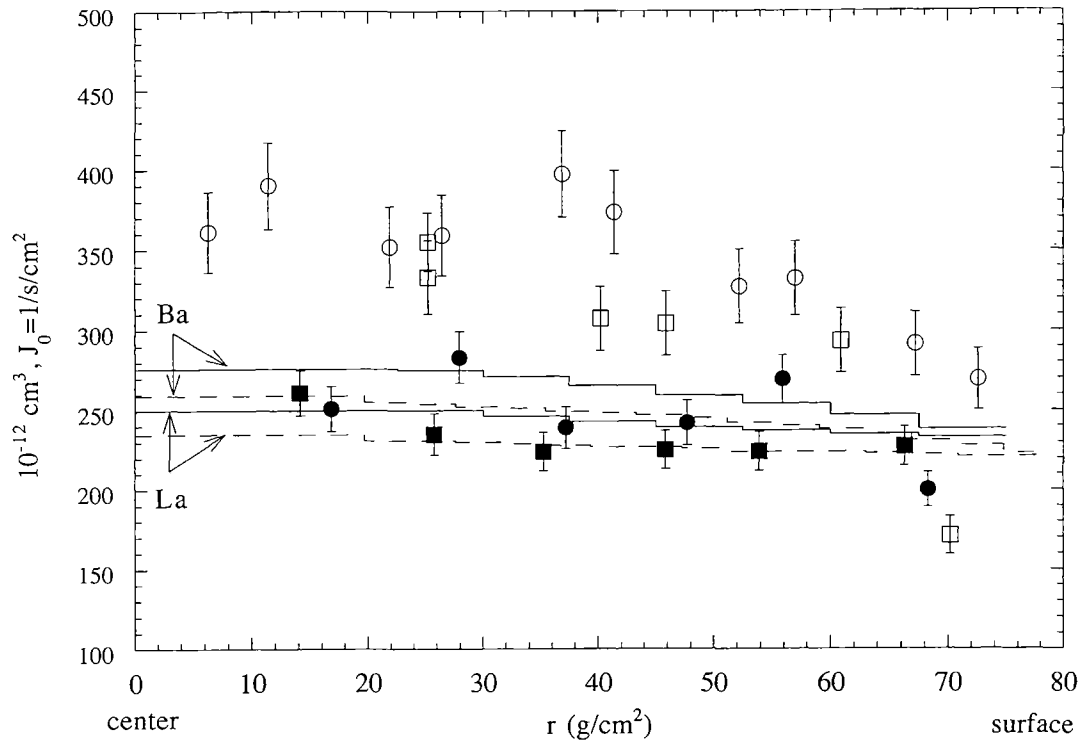


FIG. 13. Experimental and calculated ^{126}Xe production rates from barium (circles) and lanthanum (squares) are presented in units of $10^{-12} \text{ cm}^3 \text{ g}^{-1} \text{ Ma}^{-1}$ (normalised to $J_0 = 1 \text{ s}^{-1} \text{ cm}^{-2}$) in the gabbro and iron spheres irradiated at LNS vs. the distance from the center in units of g cm^{-2} . Measurements are reported using empty symbols in case of the gabbro sphere and filled symbols in case of the iron sphere. Corresponding model calculations are plotted using continuous and dashed lines, respectively.

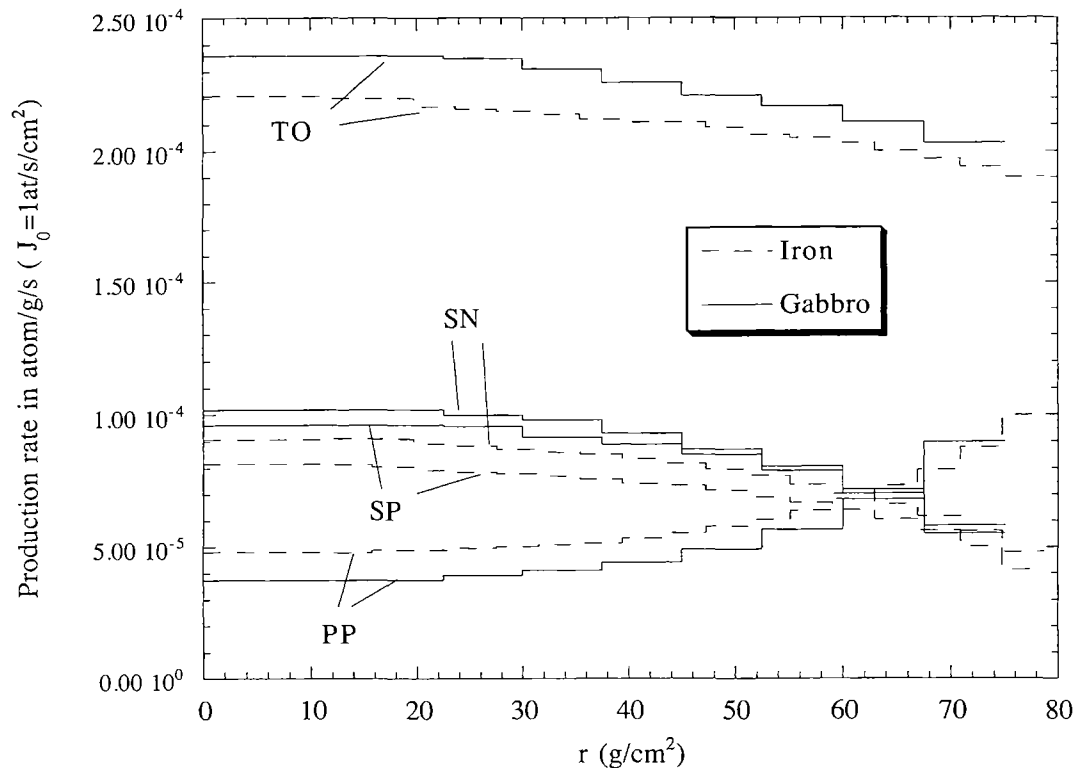


FIG. 14. Calculated ^{126}Xe production rates from barium in units of $10^{-12} \text{ cm}^3 \text{ g}^{-1} \text{ Ma}^{-1}$ (normalised to $J_0 = 1 \text{ proton s}^{-1} \text{ cm}^{-2}$) in the gabbro and iron spheres irradiated at LNS vs. the distance to the centre in units of g cm^{-2} . The total calculated production (TO) and the contributions of primary and secondary protons (PP, SP) and of secondary neutrons (SN) are shown.

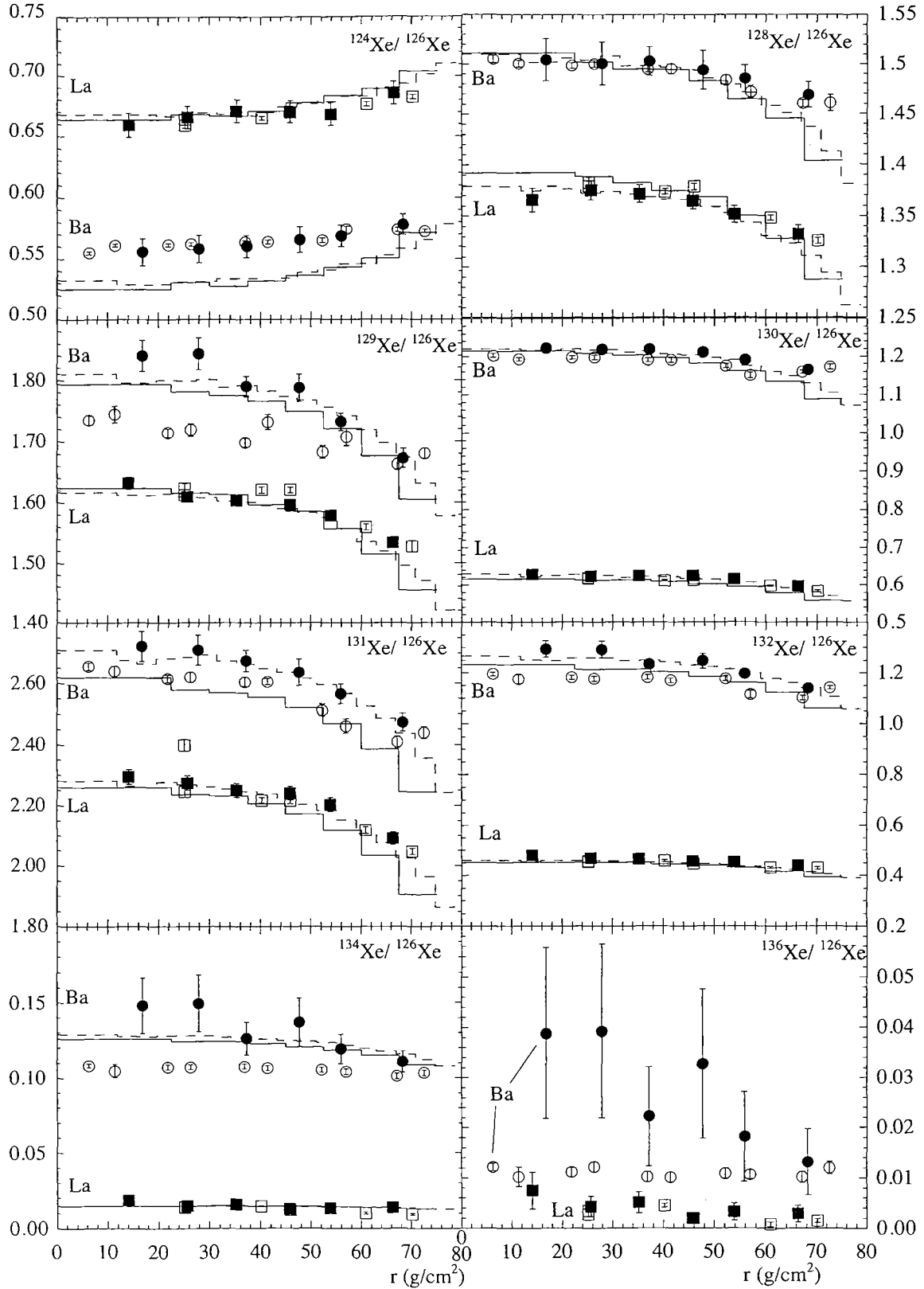


FIG. 15. Experimental and calculated Xe production rate ratios in gabbro and iron spheres irradiated with 1600 MeV protons at LNS vs. the distance from the centre in units of g cm^{-2} . The experimental results are reported using empty symbols in case of the gabbro sphere and full symbols in case of the iron sphere. Calculated production ratios are shown with solid lines for the gabbro sphere and dashed lines for the iron one.

- EBERHARDT P., EUGSTER O., GEISS J. AND MARTI K. (1966) Rare gas measurements in 30 meteorites. *Z. Naturforsch* **21a**, 414–426.
- EUGSTER O., EBERHARDT P. AND GEISS J. (1967) ^{81}Kr in meteorites and ^{81}Kr radiation ages. *Earth Planet. Sci. Lett.* **2**, 77–82.
- EUGSTER O., GEISS J., KRÄHENBÜHL U. AND NIEDERMANN S. (1986) Noble gas isotopic composition, cosmic ray exposure history, and terrestrial age of the meteorite Allan Hills A81005 from the Moon. *Earth Planet. Sci. Lett.* **78**, 139–147.
- GILABERT E., LAVIELLE B., NEUMANN S., GLORIS M., MICHEL R., SCHIEKEL TH., SUDBRÖCK F. AND HERPERS U. (1998) Cross sections for the proton-induced production of krypton isotopes from Rb, Sr, Y, and Zr for energies up to 1600 MeV. *Nucl. Instrum. Methods Phys. Res.* **B145**, 293–319.
- ISO (INTERNATIONAL ORGANISATION FOR STANDARDISATION) (1995) *ISO Guide For The Expression Of Uncertainty In Measurements*. ISO, Geneva, Switzerland.
- KINSEY R. (1979) *Data Formats and Procedures for the Evaluated Nuclear Data File ENDF*. ENDF-102, NEA Data Bank, Gif-sur-Yvette, France.
- LAVIELLE B. AND MARTI K. (1988) Cosmic-ray-produced Kr in St. Severin Core AIII. *Proc. Lunar Planet. Sci. Conf.* **18th**, 565–572.
- LAVIELLE B., SAUVAGEON H. AND BERTIN P. (1990) Cross sections for Neon and Krypton isotopes produced by neutrons. In *Workshop on Cosmogenic Nuclide Production Rates* (eds. P. A. J. Englert, R. C. Reedy and R. Michel), pp. 65–69. LPI Tech. Report **90-05**, Lunar and Planetary Institute, Houston, Texas, USA.
- LAVIELLE B., TOÉ S. AND GILABERT E. (1997) Noble gas measurements in the L/LL5 chondrite Knyahinya. *Meteorit. Planet. Sci.* **32**, 97–107.
- LEYA I. (1997) Modellrechnungen zur beschreibung der wechselwirkungen galaktischer kosmischer teilchenstrahlung mit stein- und eisenmeteoroiden, dünn-targetbestrahlungen und dick-targetexperimente. Ph.D. thesis, Universität Hannover, Germany. 459 pp.
- LEYA I. AND MICHEL R. (1997) Determination of neutron cross sections for nuclide production at intermediate energies by deconvolution of thick-target production rates. In *Nuclear Data for Science and Technology* (eds. G. Reffo, A. Ventura and C. Grandi), pp. 1463–1467. Società Italiana di Fisica, Conf. Proc. vol. **59**, Bologna, Italy.
- LEYA I. ET AL. (2000a) Simulation of the interaction of galactic cosmic-ray protons with meteoroids: On the production of radionuclides in thick gabbro and iron targets irradiated isotropically with 1.6 GeV protons. *Meteorit. Planet. Sci.* **35**, 287–318.
- LEYA I., LANGE H.-J., NEUMANN S., WIELER R. AND MICHEL R. (2000b) The production of cosmogenic nuclides in stony meteoroids by galactic cosmic-ray particles. *Meteorit. Planet. Sci.* **35**, 259–286.
- LÜPKE M. (1993) Untersuchungen zur wechselwirkung galaktischer protonen mit meteoroiden-dick-target-simulationsexperimente und messung von dünn-target-wirkungsquerschnitten. Ph.D. thesis, Universität Hannover, Germany. 260 pp.
- MARTI K. (1967) Mass-spectrometric detection of cosmic-ray-produced ^{81}Kr in meteorites and the possibility of Kr-Kr dating. *Phys. Rev. Lett.* **18**, 264–266.
- MASARIK J. AND REEDY R. C. (1994) Effects of bulk composition on nuclear production processes in meteorites. *Geochim. Cosmochim. Acta* **58**, 5307–5317.
- MATHEWS K. J., RAO M. N., WEBER H., DRAGOVITSCH P., PEIFFER F. AND MICHEL R. (1994) Xenon production cross sections at high energies and production rates of xenon isotopes in small meteorites based on simulation experiments. *Nucl. Instrum. Methods Phys. Res.* **B94**, 449–474.
- MATZKE M. (1979) Unfolding by least-squares methods: SAND-II, STAY'SL. *Proc. ASTM-Euratom Symposium on Reactor Dosimetry* **3rd**, 721–731.
- MICHEL R. AND NEUMANN S. (1998) Interpretation of cosmogenic nuclides in extraterrestrial matter on the basis of accelerator experiments and physical model calculations. *Proc. Indian Acad. Sci. (Earth Planet. Sci.)* **107**, 1–17.
- MICHEL R. ET AL. (1985) On the depth-dependence of spallation reactions in a spherical thick diorite target homogeneously irradiated by 600 MeV protons. Simulation of production of cosmogenic nuclides in small meteorites. *Nucl. Instrum. Methods Phys. Res.* **B16**, 61–82.
- MICHEL R. ET AL. (1989) Production of stable and radioactive nuclides in thick stony targets ($R = 15$ and 25 cm) isotropically irradiated with 600 MeV protons. Simulation of production of cosmogenic nuclides in meteorites. *Nucl. Instrum. Methods Phys. Res.* **B42**, 76–100.
- MICHEL R., DRAGOVITSCH P. AND FILGES D. (1990) On the dependence of cosmogenic nuclide production rates in meteoroids on bulk chemical composition (abstract). *Meteoritics* **25**, 386–387.
- MICHEL R. ET AL. (1993a) Simulation of the interaction of galactic protons with meteoroids: Isotropic irradiation of an artificial iron meteoroid with 1.6 GeV protons (abstract). *Meteoritics* **28**, 399.
- MICHEL R., LÜPKE M., HERPERS U., FILGES D., DRAGOVITSCH P., WOLFLI W., DITTRICH B. AND HOFMANN H.-J. (1993b) Simulation of the interactions of galactic cosmic-ray protons by isotropic irradiation of a thick stony target with 1.6 GeV protons. *J. Radioanal. Nucl. Chem.* **169**, 13–25.
- MICHEL R., LANGE H.-J., LÜPKE M., HERPERS U., FILGES D., CLOTH P. AND DRAGOVITSCH P. (1994) Measurement and modeling of radionuclide production in thick spherical targets irradiated isotropically with 1600 MeV protons. In *Proceedings Int. Conf. Nuclear Data for Science and Technology* (ed. J. K. Dickens), pp. 377–379. American Nuclear Society, Inc., La Grange Park, Illinois, USA.
- MICHEL R., LANGE H.-J., LÜPKE M., HERPERS U., RÖSEL R., SUTER M., DITTRICH-HANNEN B., KUBIK P. W., FILGES D. AND CLOTH P. (1995) Simulation and modeling of the interaction of galactic protons with stony meteoroids. *Planet. Space Sci.* **43**, 557–572.
- NEUMANN S. (1999) Aktivierungsexperimente mit Neutronen mittlerer Energien und die Produktion kosmogener Nuklide in extraterrestrischer Materie. Ph.D. thesis, University Hannover, Germany. 166 pp.
- PEREY F. G. (1977) *Least-Squares Dosimetry Unfolding: The Program STAY'SL*. ORNL/TM-6062, ENDF-254, NEA Data Bank, Gif-sur-Yvette, France.
- PRESCHER K., PEIFFER F., STUECK R., MICHEL R., BODEMANN R., RAO M. N. AND MATHEW K. J. (1991) Thin-target cross sections of proton-induced reactions on barium and SCR production rates of xenon-isotopes in the lunar surface. *Nucl. Instrum. Methods Phys. Res.* **B53**, 105–121.
- REGNIER S., LAVIELLE B., SIMONOFF M. AND SIMONOFF G. N. (1982) Nuclear reactions in Rb, Sr, Y, and Zr targets. *Phys. Rev.* **C26**, 931–943.